NASA Technical Memorandum 83799

NASA-TM-83799 19840027014

84-2278

Supersonic Jet Shock Noise Reduction

James R. Stone
Lewis Research Center
Cleveland, Ohio

Prepared for the
Ninth Aeroacoustics Conference
sponsored by the American Institute of Aeronautics and Astronautics
Williamsburg, Virginia, October 15–17, 1984

NASA

SUPERSONIC JET SHOCK NOISE REDUCTION

James R. Stone*
National Aeronautics and Space Administration
Lewis Research Center
Cleveland, Ohio 44135

Abstract

Shock-cell noise has been identified as a potentially significant problem for advanced supersonic aircraft at takeoff. Therefore NASA has conducted fundamental studies of the phenomena involved and model-scale experiments aimed at developing means of noise reduction. This paper reviews the results of a series of studies conducted to determine means by which supersonic jet shock noise can be reduced to acceptable levels for advanced supersonic cruise aircraft. Theoretical studies were conducted on the shock associated noise of supersonic jets from convergent-divergent (C-D) nozzles. Laboratory studies were conducted on the influence of narrowband shock screech on broadband noise and on means of screech reduction. The usefulness of C-D nozzle passages was investigated at model scale for single-stream and dual-stream nozzles. The effect of off-design pressure ratio was determined under static and simulated flight conditions for jet temperatures up to 960 K. Annular and coannular flow passages with center plugs and multielement suppressor nozzles were evaluated, and the effect of plug tip geometry was established. In addition to the far-field acoustic data, mean and turbulent velocity distributions were obtained with a laser velocimeter, and shadowgraph images of the flow field were obtained.

E-2299

Nomenclature

(All symbols are in SI units unless noted.)

A	area
c	speed of sound
D	nozzle diameter
F	functional relation
f	1/3-octave-band center frequency
h	annulus height
k	ratio of convection velocity to jet velocity
L	shock cell spacing
M	Mach number, V/c
OASPL	overall sound pressure level, dB re 20 $\mu N/m^2$
P	pressure
R	source-to-observer distance
S	nondimensional frequency parameter
SPL	1/3-octave-band sound pressure level, dB re 20 $\mu N/m^2$
T	total temperature
V	velocity
X	distance downstream of nozzle exit
α	turbulent length scale ratio
β	shock strength, $\sqrt{M_j^2 - 1}$
ρ	density
λ	wavelength
θ	polar angle from inlet axis, deg
θ_a	apparent angle of attack[25], deg
θ_M	Mach angle, $180^\circ - \sin^{-1}(1/M_j)$, deg

Subscripts:

a	ambient
c	convection
d	design point
D	downstream
e	equivalent
ef	effective
Ex	exit
h	hydraulic
ISA	international standard atmosphere (288 K and 101.3 kN/m^2)
i	inner
j	fully-expanded jet
n	shock cell number (downstream of nozzle exit)
o	outer
P	premerged
p	plug
0	aircraft
1	inner stream
2	outer stream

*Member AIAA.

Introduction

Shock-cell noise has been identified as a potentially significant problem for advanced supersonic aircraft at takeoff. Therefore, the NASA Lewis and Langley Research Centers have conducted fundamental studies of the phenomena involved and more applied studies aimed at developing means of noise reduction. Early studies indicated that it might be necessary to employ convergent-divergent (C-D) nozzle passages in order to reduce or eliminate shock noise. Some benefits have been demonstrated statically for single stream C-D circular nozzles at design jet Mach numbers of 1.5 and 2.0;[1] however, lower jet Mach numbers will probably be required to achieve acceptable jet noise levels. In addition, more complicated single- or dual-stream nozzle geometries, possibly including multielement suppressor exhaust passages will probably be required, and the effect of flight should be determined. Existing shock noise theories were found to apply to a limited degree, but only to convergent circular nozzles, thus indicating a need for further theoretical advances. Experimental data

were required to determine the degree to which these theoretical approaches could be applied to the complicated nozzle geometries and to evaluate the merit of the noise reduction concepts. This paper summarizes the results of the NASA Lewis Research Center supersonic jet shock noise reduction studies and relates these results to those of other investigators, particularly those involved in the NASA Langley Research Center Program.

A multifaceted approach was employed in the Lewis program to determine means by which supersonic jet shock noise can be reduced to acceptable levels for advanced supersonic cruise aircraft. Extensive photographic data on the flow fields of coaxial supersonic jets were obtained.[2] Theoretical studies were conducted on the shock associated noise of supersonic jets from C-D nozzles.[3,4] The influence of narrowband shock screech on broadband shock noise was investigated and means of screech reduction developed.[5-7]. The usefulness of C-D nozzle passages was investigated for single-stream[8-9] and dual-stream[10-11] nozzles. The effect of off-design pressure ratio was determined under static and simulated flight conditions for jet temperature up to 960 K. Annular and coannular flow passages with center plugs and multielement suppressor nozzles were evaluated, and the effect of plug tip geometry was established. In addition to the far-field acoustic data, mean and turbulent velocity distributions were obtained with a laser velocimeter, and shadowgraph images of the flow field were obtained. Other concepts which may prove useful for shock noise reduction are porous plug nozzles[12-13] and lined ejectors,[14] but these approaches will not be discussed in this paper.

Circular Nozzles

When a supersonic jet exhausts from a convergent circular nozzle the static pressure at the nozzle exit is above ambient. Thus, as the jet expands outside the nozzle expansion waves are radiated from the nozzle lip and are subsequently reflected by the jet boundary. These reflected compression waves converge to form a shock, again raising the jet static pressure above ambient, leading to another set of expansion waves, and the process is repeated, resulting in the familiar repetitive shock structure shown in Fig. 1. The viscous mixing taking place in the jet shear layer reduces the strength and spacing of these shock cells in the downstream direction. The eddies formed by this mixing process are convected downstream and interact with the shock cells to produce shock noise.

A very useful, although rather simplified approach to predicting shock noise for convergent circular jets was proposed by Harper-Bourne and Fisher.[15] They characterized the far-field noise as resulting from the summation of the noise generated by each eddy interacting with each shock cell as indicated by the "group" spectrum in Fig. 2. The acoustic waves from the different shocks were modeled to constructively or destructively interfere depending on the lifetime and convection velocity of the eddies, resulting in the "interference" spectrum in Fig. 2. The superposition of these results produces the characteristic spectrum of broadband shock noise, as also shown in Fig. 2. One of the major results of this model is that the broadband shock noise sound pressure level (SPL) should be proportional to $10 \log \beta^4$, where $\beta \equiv \sqrt{M_j^2 - 1}$. This same result has also been obtained theoretically, based on different reasoning by Tam et al.[3,4,16] The predicted trend is shown by the experimental results for modest values of β, as shown in Fig. 3, where the peak SPL is plotted against $10 \log \beta$ for a forward quadrant directivity angle (referred to the nozzle upstream axis, $\theta = 50°$). However, at higher values of β a Mach disc forms in the flow, reducing the strength of the downstream shocks and causing the noise levels to become relatively insensitive to further increases in β, as pointed out by Seiner and Norum.[17,18]

Influence of Screech

In addition to the broadband shock noise, discussed in the preceding section, and jet mixing noise, narrowband "screech" tones are often observed for imperfectly expanded jets. The feedback mechanism involved has been the subject of several investigations based primarily on the early work of Powell.[19] Since screech tones often produce higher SPL levels, even on a 1/3-octave-band basis, than broadband shock noise, many investigators[20-24] have used nozzle lip modifications to break the feedback loop and suppress screech in order to investigate broadband shock noise. However, the devices used to suppress screech also influenced the flow field development and consequently the broadband noise, as discussed by von Glahn.[7] This problem motivated the studies conducted by Nagel et al. to develop means of screech suppression which do not influence flow field development.[5-7]

Nagel et al.[6] devised a new method for screech tone elimination based on the feedback mechanism proposed by Powell[19] and the assumption that the acoustic waves propagating back to the nozzle exit are nearly plane waves at the nozzle exit. Under these conditions it is possible to position a reflective surface near the nozzle which establishes a local standing wave pattern from the incident and reflected screech tone. As illustrated in Fig. 4 a minimum pressure occurs at a distance of 1/4 wavelength from the reflector (and also at 3/4, 5/4, etc. wavelengths). If the reflector is positioned at the proper distance upstream of the exit, a node will occur at the nozzle exit plane (Fig. 4). This node serves to cancel the screech tone at the nozzle exit and interrupt the feedback mechanism.[6]

Although in theory a hard reflector should be used, Nagel et al.[6] obtained more consistent results with a foam disk. A comparison of spectra obtained in a reverberant room is shown in Fig. 5 for $M_j = 1.4$ with screech, with screech removed by an intrusive tab, and with screech cancelled by a foam disk located approximately 1/4 screech tone wavelength upstream of the nozzle exit. Both methods largely suppress screech. The intrusive tab however, significantly alters the broadband noise, while the foam disk does not. When screech is removed with the tab the shock cell spacing is reduced by about 10 percent, and severe distortions caused by the tab are evident in the flow and shear layer.[6] This is consistent with the results of Norum and Seiner.[23] In contrast, when the screech is removed by cancellation the flow appears unaltered from the clean nozzle case with screech.[6] Thus, it appears that where feasible, the cancellation approach is the preferred method for removing screech tones so that broadband shock noise and its suppression can be investigated.

Effect of C-D Termination

Yamamoto et al[8,9] investigated the effect of a C-D termination designed for shock-free flow at $M_j = 1.40$ (pressure ratio, $P_j/P_a = 3.12$) on circular nozzle shock noise. Experiments were conducted over a range of pressure ratios from 2.6 to 3.9, covering both overexpanded and underexpanded conditions, under static and simulated flight conditions. Results for a typical jet temperature, $T_j \simeq 960$ K, are shown in Fig. 6, where the overall sound pressure level, OASPL, is plotted against the logarithm of the shock strength parameter, β, for a forward-quadrant angle, $\theta = 50^\circ$. Data for the C-D termination are compared with data for the convergent termination. Large noise reductions can be seen in the vicinity of the C-D design point. It is an important observation that noise reductions are obtained over a wide range of pressure ratios, not just in the immediate vicinity of the design point. Directivity comparisons at the C-D design point (shown in Fig. 7) indicate that the noise reductions are obtained throughout the forward quadrant and extend somewhat into the rear quadrant. The peak noise, which should be dominated by jet mixing noise, is essentially unchanged by the C-D termination.

The spectral comparisons at the C-D design point (shown in Fig. 8) provide further insight. The C-D nozzle at its design point shows a typical jet mixing noise spectral shape with very little evidence of shock noise. Thus, it can be seen that jet mixing noise sets the "noise floor" when shock noise is suppressed. This explains the greater noise reduction, ~11 dB, in simulated flight than in the static case, ~7.5 dB, for the C-D termination, since the shock noise is amplified in flight in the forward quadrant while the jet mixing noise is generally reduced slightly (although in this particular case there is very little effect). Shadowgraph photographs and laser doppler velocimeter surveys show no evidence of shock structure for the C-D termination.

Modeling

Reasonably accurate empirical correlations of broadband shock noise for convergent circular nozzles have been obtained by several investigators[8,25] based on the Harper-Bourne and Fisher approach,[15] and theoretical[26,27] and numerical[28] models have been formulated which predict the essential features of the noise generation process. However, the interest in C-D nozzles led to the need to develop a theoretical model for the shock noise generation for off-design C-D nozzles.

Tam and Tanna[16] proposed that this noise be modeled as weak but coherent interaction between downstream propagating large turbulence structures in the mixing layer of the jet and quasi-periodic shock cells. By using simple analytical models to represent the large turbulence structures and the shock cells they derived relations for shock noise intensity scaling and peak frequency. Comparisons with their experimental data[16] were favorable, providing support for the general validity of the proposed mechanism. However, the vortex sheet model solution[16] is adequate only as a first approximation. It provides a reasonably good description of the weak shock cells in the region immediately downstream of the nozzle exit where the mixing layer is thin. Norum and Seiner[23] found that the dominant sources of shock noise lie much further downstream, near the end of the potential core, where the mixing layer is quite thick. Therefore, the vortex sheet model cannot be very accurate. Thus a better shock cell model solution which takes into account the spatial evolution of the mean flow is needed and has been developed by Tam et al.[3,4] In terms of sound level scaling, the peak SPL varies as $10 \log [(A_j/R^2)(M_j^2 - M_d^2)^2]$, as also obtained by the simpler formulation.[16] The more complete model[3,4] requires numerical computation of the peak frequency, instead of the simplified result,[16]

$$f = V_c/L(1 - M_c \cos\theta)$$

As can be seen in Fig. 9, the numerically calculated peak frequency agrees more closely than the simplified relationship with the experimental data.

These theoretical findings can be incorporated into simple empirical prediction methods, such as that of Stone and Montegani[25] rather easily. The following expression is obtained for the overall sound pressure level:

$$\mathrm{OASPL} = 162 + 10 \log \left\{ \left[\left(\frac{\rho_a}{\rho_{ISA}} \right)^2 \left(\frac{c_a}{c_{ISA}} \right)^4 \right] \right\} + 10 \log \left\{ \frac{\left(M_j^2 - M_d^2\right)^2}{1 + \left(M_j^2 - M_d^2\right)^2} \right\} + 10 \log \left(\frac{A_j}{R^2} \right) - 10 \log \left[1 - M_o \cos(\theta + \theta_a) \right] + F(\theta - \theta_M) \qquad (1a)$$

where θ_M is the Mach angle given by $180^\circ - \sin^{-1}(1/M_j)$. The function F is given by

$$F = 0 \quad \text{for} \quad \theta \le \theta_M \qquad (1a)$$

$$F = -0.75 \quad \text{for} \quad \theta > \theta_m$$

The more complicated relation than $(M_j^2 - M_d^2)^2/[1 + (M_j^2 - M_d^2)^2]$ is introduced (rather than β^4) to account for the Mach disk formation and consequent leveling off of shock noise at high β.[14,15]

The appropriate nondimensional frequency parameter, again based on the Harper-Bourne and Fisher[15] model, but also consistent with Tam and Tanna,[16] is given by

$$S = \left(\frac{fD}{kV_j} \right) \sqrt{\left| M_j^2 - M_d^2 \right|} \left[1 - M_o \cos(\theta + \theta_a) \right] \times \sqrt{\left[1 + \left(\frac{kV_j}{c_a} \right) \cos\theta \right]^2 + \alpha^2 k^2 \left(\frac{V_j}{c_a} \right)^2} \qquad (2)$$

Note that the convection velocity factor $k = 0.7$, and the turbulence length scale factor $\alpha = 0.2$.

The shock noise peaks at $S = 1.0$ and varies with log S (as shown in Fig. 10).

Annular Plug Nozzles

The experimental configurations of Yamamoto et al.[8,9] included an annular plug nozzle with both convergent and convergent-divergent terminations (as shown in Fig. 11). The annular radius ratio at the throat was 0.85. Experiments were also conducted with screech tabs on the convergent configuration.

Influence of Screech

A limited study was conducted on screech and the usefulness of tabs in reducing screech, along with the resulting effects on broadband noise. Narrowband data at $\theta = 60^\circ$ obtained with and without tabs are compared in Fig. 12, for a pressure ratio, $P_j/P_a \simeq 3.4$ and jet temperature, $T_j \simeq 483$ K. A strong discrete tone at 937.5 Hz is apparent for the nozzle without tabs and is barely discernible with tabs. In addition the broadband shock noise is somewhat reduced in level and shifted to a higher frequency with tabs. The corresponding 1/3-octave-band spectra are shown in Fig. 13(a), and it can be seen that the tabs influence a fairly wide frequency range. The shift of the broadband peak cannot be seen because the spectrum without tabs is so strongly influenced by screech that the broadband peak cannot be determined. The corresponding aft quadrant spectra at $\theta = 140^\circ$ are shown in Fig. 13(b). The screech tabs produce a noise reduction over the entire spectrum, even though jet mixing noise is the dominant source at this angle. It is clear from these results that the tabs influence the mixing process as well as break the feedback loop. At higher temperature, $T_j \simeq 960$ K, the screech is weaker and the influence of the tabs is less than at the lower temperature (as shown in Fig. 14). From these comparisons it appears that the high-temperature data without tabs are the most valid broadband shock noise data, since the influence of screech is fairly small, whereas the tabs have a noticeable effect on the flow field. The foam disc cancellation approach was not considered practical for these tests because of the inclusion of simulated flight testing.

Effect of C-D Termination

Yamamoto et al.[8,9] investigated the effect of a C-D termination designed for shock-free flow at $M_j = 1.44$ (pressure ratio, $P_j/P_a = 3.30$) on shock noise for an annular plug nozzle with a throat radius ratio of 0.85. The exit radius ratio of the C-D nozzle was 0.79. Experiments were conducted over a range of pressure ratios from 2.94 to 3.54, covering both over-expanded and under-expanded conditions, under static and simulated flight conditions. Results for a typical jet temperature, $T_j \simeq 960$ K, are shown in Fig. 15, where the OASPL is plotted against $\log \beta$ for a forward-quadrant angle, $\theta = 50^\circ$. Data for the C-D termination are compared with data for the convergent termination and with data for the baseline convergent circular nozzle. Perhaps the most significant observation is that the C-D termination does not provide any significant reduction in noise compared with the convergent annular plug nozzle, although both annular plug nozzles provide suppression, ~6 dB, relative to the baseline convergent circular nozzle. Directivity comparisons shown in Fig. 16 and spectral comparisons at $\theta = 50^\circ$ (shown in Fig. 17) support this observation.

The reason for the ineffectiveness of the C-D termination is that, as shown by laser velocimeter (LV) measurements, near the C-D design point both the convergent and C-D nozzles produce shocks downstream of the plug, and the shock noise generated in that region exceeds that generated in the plug region. As the LV results also showed, even though shocks on the plug were eliminated by the C-D termination, the plume velocity at the plug tip was still supersonic. Consequently the truncated plug tip produces a series of expansion and shock waves downstream which interact with the turbulent mixing layer to produce shock noise.[8] From the spectral comparisons in Fig. 17, it can be seen that the C-D termination does provide some noise reduction at high frequency, which is attributable to the suppression of shock noise in the plug region. However, in the aft quadrant the directivity comparisons of Fig. 16 indicate that the C-D termination produces increased noise; this result is consistent with the reduction in nozzle exit radius ratio.

Effect of Plug Tip Geometry

The tests of Yamamoto et al.[8,9] did not include the effects of plug tip geometry. However, Janardan, Yamamoto et al.[10,11] investigated the effect of plug tip geometry for a dual-stream coannular plug nozzle. The downstream-generated shock noise was substantially reduced when a sharp tipped plug was used instead of a truncated plug. This effect should also be observed for the single-stream annular plug nozzle.

Modeling

For purposes of predictive modeling, annular plug nozzle shock noise is broken into two components: noise generated in the premerged region in the vicinity of the plug, and noise generated downstream of the plug, as shown by Yamamoto et al.[8] This is illustrated in Fig. 18, where the spectra at $\theta = 50^\circ$ for both the convergent and C-D termination are compared with each other and with predictions based on modified inputs to the Motsinger-Sieckman (M-S) model[29] (which is based on Harper-Bourne and Fisher[15]). The aerodynamic conditions correspond to the C-D design point. At low and middle frequencies the two annular nozzles show little difference and agree well in spectral shape with predictions taking the effective diameter to be the nozzle equivalent diameter, $D_e = \sqrt{4A_j/\pi}$. (The level is arbitrary.) This noise is therefore ascribed to the downstream region.

In the high frequency region the convergent nozzle levels exceed those of C-D configuration, which indicates that this noise is generated in the plug region, where the C-D nozzle has no shocks. The spectral shape agrees with the M-S model[29] using the hydraulic diameter, $D_h = 4A/\pi D_o$, as the effective diameter.

Plug region. A theoretical study of shock noise generation in this region was conducted by Balsa,[8] based on extension of the Howe and Ffowcs Williams[26] model. Balsa found that the SPL should increase with $10 \log \beta^4$ as predicted by other models. He also found a directional dependence, SPL $\propto 10 \log (1 - M_c \cos \theta)$ as also found by Howe

and Ffowcs Williams[26] but which is not found in predictions based on the Harper-Bourne and Fisher model.[15] However, because of the difficulty in separating out the effect of high frequency jet mixing noise, it is uncertain whether this rather weak directivity is actually present.

The observations of Yamamoto et al.[8] can be incorporated into simple empirical prediction methods, such as the circular nozzle model proposed earlier in this paper, which is based on that of Stone and Montegani[25] (which, in turn, is based on Harper-Bourne and Fisher[15]). In order to get proper limiting behavior with a two-source model, the constant in Eq. (1) must be reduced by 3 dB. An additional level correction is also required; the form $\Delta SPL \propto \log [1 - (D_i/D_o)_{Ex}]$ gives the proper limiting behavior, and the proportionality constant is about 10. The following expression is then obtained for the overall sound pressure level:

$$OASPL_p = 159 + 10 \log \left[\left(\frac{\rho_a}{\rho_{ISA}}\right)^2 \left(\frac{c_a}{c_{ISA}}\right)^4\right] + 10 \log \left[1 - \left(\frac{D_i}{D_o}\right)_{Ex}\right] + 10 \log \left(\frac{A_j}{R^2}\right) + 10 \log \left\{\frac{\left(M_j^2 - M_d^2\right)^2}{1 - \left(M_j^2 - M_d^2\right)^2}\right\} + 10 \log \left[1 - M_o \cos (\theta + \theta_a)\right] + F(\theta - \theta_M) \quad (3)$$

where $F(\theta - \theta_M)$ is given by Eq. (1a). The appropriate nondimensional frequency parameter, to be used in conjunction with Fig. 10, is given by

$$S_p = \left(\frac{fD_h}{0.7\ V_j}\right) \sqrt{\left|M_j^2 - M_d^2\right|} \left[1 - M_o \cos (\theta + \theta_a)\right] \times \sqrt{\left[1 + 0.7 \left(\frac{V_j}{c_a}\right) \cos \theta\right]^2 + 0.0196 \left(\frac{V_j}{c_a}\right)^2} \quad (4)$$

Downstream region. Again the observations of Yamamoto et al.[8] are incorporated into the model of Stone and Montegani[25], and limiting behavior is taken into account. The following expression is then obtained for the OASPL:

$$OASPL_D = 159 + 10 \log \left[\left(\frac{\rho_a}{\rho_{ISA}}\right)^2 \left(\frac{c_a}{c_{ISA}}\right)^4\right] + 10 \log \left(\frac{A_j}{R^2}\right) + 10 \log \left\{\frac{\left[M_j^2 - M_{d,p}^2\right]^2}{1 + \left(M_j^2 - M_{d,p}^2\right)^2}\right\} - 10 \log \left[1 - M_o \cos (\theta + \theta_a)\right] + F(\theta - \theta_M) \quad (5)$$

where $F(\theta - \theta_M)$ is given by Eq. (1a), and $M_{d,p}$ is equal to the design Mach number if an extended plug is used and is 1.0 if a truncated plug is used. The appropriate nondimensional frequency parameter, to be used in conjunction with Fig. 10, is given by

$$S_D = \left(\frac{fD_e}{0.7\ V_j}\right) \sqrt{\left|M_j^2 - M_{d,p}^2\right|} \left[1 - M_o \cos (\theta + \theta_a)\right] \times \sqrt{\left[1 + 0.7 \left(\frac{V_j}{c_a}\right) \cos \theta\right]^2 + 0.0196 \left(\frac{V_j}{c_a}\right)^2} \quad (6)$$

Coannular Nozzles

Most modern jet engines are of the dual-stream type and have coannular exhaust nozzles. Therefore, information on the noise characteristics of such nozzles is quite important. The dual-stream shock noise studies of Janardan, Yamamoto et al.[10,11] included convergent and C-D coannular plug nozzles with both truncated and extended plugs (as shown in Fig. 19). Both the coannular nozzles had an inner-stream radius ratio of 0.93 and an outer-stream radius ratio of 0.85.

Influence of Screech

Since screech was shown by Yamamoto et al.[8] to be less for an annular nozzle than for a circular nozzle and to decrease with increasing temperature, it was not expected to be a critical problem in these experiments, particularly at jet temperatures of practical interest. The narrowband spectra shown in Fig. 20 confirm this expectation. Moderate levels of screech are seen at moderate temperatures under both static (Fig. 20(a)) and simulated flight (Fig. 20(b)) conditions. The higher temperature spectra shows some evidence of screech (at ~1200 Hz) under static conditions (Fig. 20(c)) but none in simulated flight (Fig. 20(d)). Thus, it is concluded that screech is not a critical problem, but care must be exercised in analyzing the data, especially for temperature effects.

Effect of Temperature

The effect of outer-stream temperature for the convergent coannular nozzle is shown in Fig. 21. OASPL directivities are shown for two different outer-stream temperatures under both static (Fig. 21(a)) and simulated flight (Fig. 21(b)) conditions. The increased aft quadrant noise at high temperature is due to increased jet mixing noise. In the forward quadrant the reverse effect is seen, but is of relatively small magnitude. This increase at lower temperature is probably due largely to the increased screech, and the broadband shock noise is relatively insensitive to temperature.

Effect of C-D Termination

Janardan, Yamamoto et al.[10,11] investigated the effect of C-D terminations designed for shock-free flow at an inner-stream Mach number, $M_{j,1} = 1.38$, and an outer-stream Mach number, $M_{j,2} = 1.44$. At the exit the inner-stream radius ratio was 0.91, and that of the outer-stream was 0.79. Experiments were conducted over a range of over-expanded and under-expanded conditions for both streams, under

static and simulated flight conditions. Typical results for the truncated plug are shown in Fig. 22, where the OASPL is plotted against 10 log β_{ef} for a forward-quadrant angle, $\theta = 60^\circ$. (The effective shock strength, β_{ef}, is calculated from an area-weighted pressure ratio, as defined subsequently in the "Modeling" discussion.) Data for the C-D configuration are compared with data for the convergent coannular nozzle; also shown for comparison are baseline convergent circular nozzle data scaled to the fully-mixed conditions of the dual-stream nozzles. It can be seen that at the C-D design point the C-D nozzle provides about 2 dB reduction under static conditions and about 5 dB reduction in simulated flight relative to the convergent coannular nozzle. The convergent coannular nozzle itself provides about 5 dB reduction under static conditions and about 6 dB reduction in simulated flight relative to the fully-mixed convergent circular nozzle.

OASPL comparisons for these configurations at the C-D design point are shown in Fig. 23. The C-D termination is seen to reduce noise throughout the forward quadrant. The noise increase in the aft quadrant with the C-D termination is due to the effect of the decreased radius ratios at the exit. The corresponding forward quadrant spectral comparisons at $\theta = 60^\circ$ are shown in Fig. 24. Broadband shock noise is clearly present even with the C-D terminations, but its level is reduced, with little or no frequency shift. The significant residual shock noise with the C-D configuration will be shown to be due to plug tip geometry.

Effect of Plug Tip Geometry

Because of the residual shock noise observed for annular[8] and coannular[10] nozzles with truncated plugs, Janardan et al.[10] investigated the effect of plug tip geometry. Typical results are shown in Fig. 25, where the OASPL is plotted against 10 log β_{ef} for a forward quadrant angle, $\theta = 60^\circ$. Data for the nozzle with C-D terminations and an extended plug are compared with both the C-D coannular nozzle with truncated plug and the convergent coannular nozzle with truncated plug. It can be seen that the extended plug provides an additional 1.5 dB (static) to 3 dB (simulated flight) suppression relative to the C-D nozzle with truncated plug. Compared to the convergent nozzle with truncated plug, the C-D nozzle with extended plug provides 2.5 dB suppression under static conditions and 7 dB under simulated flight conditions.

OASPL directivity comparisons at the C-D design point are shown in Fig. 26. The extended plug is seen to provide additional noise reduction throughout the forward quadrant and has no significant effect in the rear quadrant, where jet mixing noise is dominant. The corresponding forward quadrant spectral comparisons at $\theta = 60^\circ$ are shown in Fig. 27. It appears that there may be some shock noise still present with the extended plug, but if so its contribution is relatively small.

Effect of Subsonic Inner Stream

Some candidate engine cycles for advanced supersonic transports feature coannular exhausts with a supersonic outer stream and subsonic inner stream (e.g., Refs. 2, 22, and 30 to 33). Therefore, Janardan, Yamamoto et al.[10,11] conducted experiments at such conditions for the convergent coannular nozzle with the extended plug. The effect of the subsonic inner stream conditions is illustrated in Fig. 28, where the OASPL is plotted against 10 log β_{ef} for a forward quadrant angle, $\theta = 60^\circ$, for the convergent coannular nozzle at subsonic and supersonic inner stream conditions. The subsonic inner stream provides a significant noise reduction over a range of effective Mach number from 1.35 to 1.5 in simulated flight and over a wider range under static conditions. OASPL directivity comparisons are shown in Fig. 29 for an effective jet Mach number of ~1.4, where the beneficial effect of the subsonic inner stream is most pronounced. The subsonic inner stream provides a noise reduction throughout the forward quadrant. Near the jet axis where jet mixing noise is predominant, there is no significant change. The corresponding spectral comparisons at $\theta = 60^\circ$ are shown in Fig. 30. A significant reduction in broadband shock noise is quite evident. These results are consistent with diagnostic LV measurements, which indicated a significant weakening of the shock structure with a subsonic inner stream.

Modeling

For purposes of predictive modeling, coannular plug nozzle shock noise is broken into two components, like the annular plug nozzle: noise generated in the vicinity of the plug, and noise generated downstream of the plug, as shown by Janardan et al.[10] Janardan developed modifications to the Harper-Bourne and Fisher approach[12] to account for his findings, which are now applied to the Stone and Montegani model[25] using a similar approach to that used for the annular plug model.

Plug region. Since the shocks on the plug are due mainly to the outer stream expansion, the prediction is based on outer stream conditions. The following expression, derived from Eq. (3), is then obtained for the overall sound pressure level:

$$\begin{aligned} OASPL_p = 159 &+ 10 \log \left[\left(\frac{\rho_a}{\rho_{ISA}} \right)^2 \left(\frac{c_a}{c_{ISA}} \right)^4 \right] \\ &+ 10 \log \left[1 - \left(\frac{D_{i,2}}{D_{o,2}} \right)_{Ex} \right] + 10 \log \left(\frac{A_j}{R^2} \right) \\ &+ 10 \log \left\{ \frac{\left[M_{j,2}^2 - M_{d,2}^2 \right]^2}{1 - \left(M_{j,2}^2 - M_{d,2}^2 \right)^2} \right\} \\ &- 10 \log \left[1 - M_o \cos (\theta + \theta_a) \right] \\ &+ F(\theta - \theta_{M,2}) \end{aligned} \qquad (7)$$

The appropriate nondimensional frequency parameter, to be used in conjunction with Fig. 10, is given by

$$S_p = \left(\frac{f D_{h,2}}{0.7\, V_j} \right) \sqrt{\left| M_{j,2}^2 - M_{d,2}^2 \right|} \left[1 - M_o \cos (\theta + \theta_a) \right] \times \sqrt{\left[1 + 0.7 \left(\frac{V_{j,2}}{c_a} \right) \cos \theta \right]^2 + 0.0196 \left(\frac{V_j}{c_a} \right)^2} \qquad (8)$$

Downstream region. Janardan[10] showed that the downstream shock noise depends on the conditions of both streams in a rather complicated manner. The effective pressure ratio is given by the appropriate relation, as follows:

$$\frac{P_{j,ef}}{P_a} = \frac{P_{j,1}}{P_a} \quad \text{for} \quad P_{j,1} \geq P_{j,2} \tag{9a}$$

$$\frac{P_{j,ef}}{P_a} = \frac{P_{j,1}}{P_a}\left[\frac{A_{j,1}}{A_{j,1} + A_{j,2}} + \frac{A_{j,2}P_{j,2}}{P_{j,1}\left(A_{j,1} + A_{j,2}\right)}\right] \tag{9b}$$

$$\text{for} \quad P_{j,1} < P_{j,2}$$

Using the fully-mixed jet total temperature, the effective Mach number, $M_{j,ef}$, is calculated along with the effective jet velocity, $V_{j,ef}$. The values are then substituted, along with total area, $A_{j,1} + A_{j,2}$, into Eqs. (5) and (6). The resulting expression for OASPL is then given by

$$\begin{aligned} OASPL_D = {} & 159 + 10 \log \left[\left(\frac{\rho_a}{\rho_{ISA}}\right)^2 \left(\frac{c_a}{c_{ISA}}\right)^4\right] \\ & + 10 \log \left[\frac{\left(A_{j,1} + A_{j,2}\right)}{R^2}\right] \\ & + 10 \log \left\{\frac{\left[M_{j,ef}^2 - M_{d,p}^2\right]^2}{1 + \left(M_{j,ef}^2 - M_{d,p}^2\right)^2}\right\} \\ & - 10 \log \left[1 - M_o \cos\left(\theta + \theta_a\right)\right] \\ & + F(\theta - \theta_{M,ef}) \end{aligned} \tag{10}$$

where $M_{d,p}$ is calculated by substituting the design conditions into Eq. (9) and taking the resulting Mach number as the effective $M_{d,p}$ for the extended plug case, or by setting $M_{d,p} = 1$ for a truncated plug. The appropriate nondimensional frequency parameter, to be used in conjunction with Fig. 10 is given by

$$\begin{aligned} S_D = {} & \left(\frac{fD_e}{0.7\, V_{j,ef}}\right) \\ & \times \sqrt{\left|M_{j,ef}^2 - M_{d,p}^2\right|}\ \left[1 - M_o \cos\left(\theta + \theta_a\right)\right] \\ & \times \sqrt{\left[1 + 0.7\left(\frac{V_{j,ef}}{c_a}\right)\cos\theta\right]^2 + 0.0196\left(\frac{V_{j,ef}}{c_a}\right)^2} \end{aligned} \tag{11}$$

where D_e is based on the total nozzle area. Instead of using formulations of this type for the C-D termination effect, Janardan calculated the noise for $M_{d,p} = 1$ and developed a set of empirical corrections.[10] No comparison has yet been made to determine the differences between these two approaches.

Multielement Suppressors

Multielement suppressor nozzles may very well be required to provide sufficiently low jet mixing noise for advanced supersonic transports.[14,33-37] When a multielement nozzle is used to suppress jet mixing noise, the shock noise can become a more important source relative to jet mixing noise. Therefore, shock noise reduction for suppressors is of interest. Both single-stream[8] and outer-stream (in a dual-stream exhaust)[10] suppressors were investigated. Because of the complicated nozzle exit geometries, no strong feedback loop is established, and screech is not an important factor. Because of the rapid mixing with these nozzles, no significant effect of plug tip geometry is expected.

Effect of C-D Termination

The effect of C-D termination of the nozzle elements was investigated for both single-stream[8] and dual-stream[10] nozzles.

Single-stream. Yamamoto et al.[8,9] investigated the effect of C-D suppressor elements, designed for shock-free flow at $M_j = 1.42$, on a 20-chute annular plug suppressor nozzle (Fig. 31), having a suppressor area ratio of 1.75 and radius ratio of 0.76 at the throat. Results for a typical jet temperature, $T_j = 950$ K (shown in Fig. 32) where the OASPL is plotted against 10 log β for a forward quadrant angle, $\theta = 50°$. Data for the C-D terminations are compared with data for the convergent terminations and with data for the baseline convergent circular nozzle. The C-D elements clearly provide additional shock noise suppression beyond that provided by the convergent suppressor in the simulated flight case. Corresponding spectral comparisons at the C-D design conditions (shown in Fig. 33) show the C-D elements effectively suppress the shock noise, which peaks at 1250 Hz. However, at middle frequencies the C-D elements produce some increase in noise. OASPL directivity comparison at these conditions (shown in Fig. 34) and aft-quadrant spectral comparisons at $\theta = 140°$ (shown in Fig. 35) clarify the situation. In the aft quadrant jet mixing noise is dominant, and the C-D suppressor is significantly noisier than the convergent suppressor. Laser velocimeter measurements confirm the expectation that the weakened shocks produce less rapid mixing and, consequently, more jet noise. This is not surprising since one method of enhancing jet mixing and noise reduction is to promote a strong normal shock near the nozzle.[2,34]

Dual-stream. Janardan, Yamamoto et al.[10,11] investigated the effect of C-D suppressor elements and C-D inner-stream nozzle on a 20-chute outer-stream suppressor coannular plug nozzle shown in Fig. 36. The suppressor area ratio was 1.75, and the suppressor radius ratio was 0.76 at the throat; the inner-stream nozzle had a radius ratio at the throat of 0.94 and an area constituting 0.2 of the total exit area. Results for typical conditions are shown in Fig. 37, where OASPL is plotted against 10 log β_{ef} for a forward quadrant angle, $\theta = 60°$. Data for the C-D terminations are compared with data for the convergent terminations and with data for the baseline convergent circular nozzle at fully-mixed dual-stream conditions. The effect of the C-D terminations is that the C-D

elements provide no additional shock noise OASPL suppression beyond that of a convergent suppressor, although perceived noise levels (not shown) are slightly reduced. The effect of C-D terminations on the SPL spectra (shown in Fig. 38) and the OASPL directivity (shown in Fig. 39) illustrate the same general effects as for the single-stream suppressor: while there is some reduction in shock noise, especially downstream, the jet mixing noise is increased. Thus it appears that while C-D suppressor elements may reduce shock noise, they may not be practical for aircraft applications because of the increased jet mixing noise.

Modeling

For purposes of predictive modeling, the shock noise generation for the suppressor nozzle is broken into two components: premerged noise generated near the nozzle exit where the individual elements of the flow are discernible, and the noise generated in the downstream mixing region.

Single-stream suppressors. Because of the rapid mixing of the flow elements with downstream distance, the downstream region is subsonic and there is no downstream shock noise generation. Yamamoto et al.[8] compared the experimental results with predictions based on modified inputs to the M-S model.[29] Reasonable agreement was found using D_h as the characteristic dimension. Thus Eqs. (3) and (4) should be appropriate, where D_h is the element hydraulic diameter, and D_i and D_o are the inside and outside diameters, respectively of circles intersecting the innermost and outermost positions of the suppressor elements.

Dual-stream suppressors. The same approach should be applicable for premerged shock noise as used for the single-stream suppressor. Therefore, Eqs. (7) and (8) should be appropriate. For the downstream region, only the inner stream should contribute because of the rapid mixing of the outer stream. Applying this reasoning, we obtain

$$OASPL_D = 159 + 10 \log \left[\left(\frac{\rho_a}{\rho_{ISA}}\right)^2 \left(\frac{c_a}{c_{ISA}}\right)^4\right] + 10 \log \left(\frac{A_{j,1}}{R^2}\right) + 10 \log \left\{\frac{\left(M_{j,1}^2 - M_{d,1}^2\right)^2}{1 + \left(M_{j,1}^2 - M_{d,1}^2\right)^2}\right\} - 10 \log \left[1 - M_o \cos\left(\theta + \theta_a\right)\right] + F(\theta - \theta_{M,1}) \quad (12)$$

The appropriate nondimensional frequency parameter, to be used in conjunction with Fig. 10 is given by

$$S_D = \left(\frac{fD_{e,1}}{0.7\, V_{j,1}}\right) \times \sqrt{\left|M_{j,1}^2 - M_{d,1}^2\right|}\, \left[1 - M_o \cos\left(\theta + \theta_a\right)\right] \times \sqrt{\left[1 + 0.7\left(\frac{V_{j,1}}{c_a}\right)\right]^2 + 0.0196\left(\frac{V_{j,1}}{c_a}\right)^2} \quad (13)$$

Conclusions

The most important result of these studies is that supersonic jet shock noise can be reduced by proper C-D design of nozzle flow passages and center plugs, even for the complicated nozzle geometries investigated experimentally. Furthermore, the noise reduction is obtained over a fairly wide range of pressure ratios above and below the C-D shock-free design point. This finding was predicted theoretically for the single-stream circular C-D nozzle and also found experimentally to be true for the more complicated geometries. However, it was found that the shock noise reductions were generally accompanied by some increase in jet mixing noise (except for the circular nozzle); this effect was especially pronounced for the suppressor nozzles. Thus, it is clear that tradeoffs will be required in applying the C-D nozzle approach to noise reduction in most practical situations, where jet mixing noise must also be considered.

References

1. Seiner, J. M., and Norum, T. D., "Experiments on Shock Associated Noise of Supersonic Jets," AIAA Paper 79-1526, July 1979.

2. Dosanjh, D. S., and McAfee, R. S., Jr., "Coaxial Supersonic Jet Flow Shock Structure and Related Limitations of Comparative Noise Suppression Assessment Schemes," AIAA Paper 83-0707, April 1983.

3. Tam, C. K. W., and Jackson, J. A., "On Shock Cell Structure and Noise of Supersonic Jets," AIAA Paper 83-0703, April 1983.

4. Tam, C. K. W., "On the Shock Cell Structure and Noise of Supersonic Jets," Proc. 11th International Conference on Acoustics, Vol. I, Paris, France, July 1983, pp. 333-336.

5. Nagel, R. T., and Papathanasiou, A. G., "An Experimental Study of Supersonic Jet Shock Associated Noise," AIAA Paper 83-0708, April 1983.

6. Nagel, R. T., Denham, J. W., and Papathanasiou, A. G., "Supersonic Jet Screech Tone Cancellation," AIAA J., Vol. 21, No. 11, Nov. 1983, pp. 1541-1545.

7. von Glahn, U., "New Interpretations of Shock-Associated Noise With and Without Screech," NASA TM-81590, 1980.

8. Yamamoto, K., Brausch, J. F., Balsa, T. F., Janardan, B. A., and Knott, P. R., "Experimental Investigation of Shock-Cell Noise Reduction for Single Stream Nozzles in Simulated Flight," to be published NASA Contractor Report.

9. Yamamoto, K., Brausch, J. F., Janardan, B. A., Hoerst, D. J., Price, A. O., and Knott, P. R., "Experimental Investigation of Shock-Cell Noise Reduction for Single-Stream Nozzles in Simulated Flight, Comprehensive Data Report, Volumes I-III," General Electric Co. Report R82AEB491, May 1984. (NASA CR-168234)

10. Janardan, B. A., Yamamoto, K., Majjigi, R. K., and Brausch, J. F., "Experimental Investigation of Shock-Cell Noise Reduction for Dual-Stream Nozzles in Simulated Flight," to be published NASA Contractor Report.

11. Yamamoto, K., Janardan, B. A., Brausch, J. F., Hoerst, D. J., and Price, A. O., "Experimental Investigation of Shock-Cell Noise Reduction for Dual-Stream Nozzles in Simulated Flight, Comprehensive Data Report, Volumes I-II," General Electric Co. Report R83AEB358, Feb. 1984. (NASA CR-168336)

12. Maestrello, L., "An Experimental Study on Porous Plug Jet Noise Suppressor," AIAA Paper 79-0673, Mar. 1979.

13. Bauer, A. B., "Jet Noise Suppression by Porous Plug Nozzles," AIAA Paper 81-1993, Oct. 1981.

14. FitzSimmons, R. D., McKinnon, R. A., and Johnson, E. S., "Flight and Tunnel Test Results of the MDC Mechanical Jet Noise Suppressor Nozzle," Supersonic Cruise Research '79, Part I, NASA CP-2108, 1980, pp. 453-478.

15. Harper-Bourne, M., and Fisher, M. J., "The Noise from Shock Waves in Supersonic Jets," Noise Mechanisms, AGARD-CP-131, Mar. 1974, pp 11-1 to 11-13.

16. Tam, C. K. W., and Tanna, H. K., "Shock Associated Noise of Supersonic Jets from Convergent-Divergent Nozzles," J. Sound Vibration, Vol. 81, 1982, pp. 337-358.

17. Seiner, J. M., and Norum, T. D., "Experiments on Shock Associated Noise of Supersonic Jets," AIAA Paper 79-1526, July 1979.

18. Seiner, J. M., and Norum, T. D., "Aerodynamic Aspects of Shock Containing Jet Plumes," AIAA Paper 80-0965, June 1980.

19. Powell, A., "On the Mechanism of Choked Jet Noise," Proc. Phys. Soc., Sec. B., Vol. 66, 1953, pp. 1039-1056.

20. Tester, B. J., Morris, P. J., Lau, J. C., and Tanna, H. K., "The Generation, Radiation and Prediction of Supersonic Jet Noise," AFAPL-TR-78-85-Vol. 1, Oct. 1978.

21. Tanna, H. K., "An Experimental Study of Jet Noise, Part II: Shock Associated Noise," J. Sound Vibration, Vol. 50, No. 3, 1977, pp. 429-444.

22. Kozlowski, H., and Packman, A. B., "Flight Effects on the Aerodynamic and Acoustic Characteristics of Inverted Profile Coannular Nozzles," NASA CR-3018, 1978.

23. Norum, T. D., and Seiner, J. M., "Broadband Shock Noise from Supersonic Jets," AIAA J., Vol. 20, 1982, pp. 68-73 (AIAA Paper 80-0983).

24. Norum, T. D., "Screech Suppression in Supersonic Jets," AIAA Paper 82-0050, Jan. 1982.

25. Stone, J. R., and Montegani, F. J., "An Improved Prediction Method for the Noise Generated in Flight by Circular Jets," NASA TM-81470, 1980.

26. Howe, M. S., and Ffowcs-Williams, J. E., "On the Noise Generated by an Imperfectly Expanded Supersonic Jet," Phil. Trans. Roy. Soc. London, Vol. A289, No. 1358, 1978, pp. 271-314.

27. Pao, S. P., and Seiner, J. M., "A Theoretical and Experimental Investigation of Shock Associated Noise in Supersonic Jets," AIAA Paper 81-1973, Oct. 1981

28. Pao, S. P., and Salas, M. D., "A Numerical Study of Two-Dimensional Shock Vortex Interaction," AIAA Paper 81-1205, June 1981.

29. Gliebe, P. E., Motsinger, R. E., and Sieckman, A., "High Velocity Jet Noise Source Location and Reduction, Task 6 Supplement - Computer Programs," FAA-RD-78-79, Vol. 1a, Mar. 1979.

30. Tanna, H. K., Tam, C. K. W., and Brown, W. H., "Shock Associated Noise Reduction from Inverted-Velocity-Profile Coannular Jets," Lockheed Report No. LG81ER0162, Aug. 1981. (NASA-CR-3454)

31. Stone, J. R., "An Empirical Model for Inverted-Velocity-Profile Jet Noise Prediction," NASA TM-73838, 1977.

32. Goodykoontz, J. H., and Stone, J. R., "Experimental Study of Coaxial Nozzle Exhuast Noise," AIAA Paper 79-0631, Mar. 1979. (NASA TM-79090)

33. Stone, J. R., Goodykoontz, J. H., and Gutierrez, O. A., "Effects of Geometric and Flow-Field Variables on Inverted-Velocity-Profile Coaxial Noise and Source Distributions," AIAA Paper 79-0635, Mar. 1979. (NASA TM-79095)

34. Huff, R. G., and Groesbeck, D. E., "Cold-Flow Acoustic Evaluation of a Small-Scale, Divergent, Lobed Nozzle for Supersonic Jet Noise Suppression," NASA TM-X-3210, 1975.

35. Simcox, C. D., Armstrong, R. S., and Atvars, J., "Recent Advances in Exhaust Systems for Jet Noise Suppression of High Speed Aircraft," J. Aircraft, Vol. 13, No. 6, June 1976, pp. 442-448.

36. Stone, J. R., Miles, J. H., and Sargent, N. B., "Effects of Forward Velocity on Noise for a J85 Turbojet Engine with Multi-Tube Suppressor from Wind Tunnel and Flight Tests," NASA TM-X-73542, 1976.

37. Moore, M. T., "Flight Effects on the Jet Noise Signature of a 32-Chute Suppressor Nozzle as Measured in the NASA Ames 40x80 Foot Wind Tunnel," NASA CR-152175, 1979.

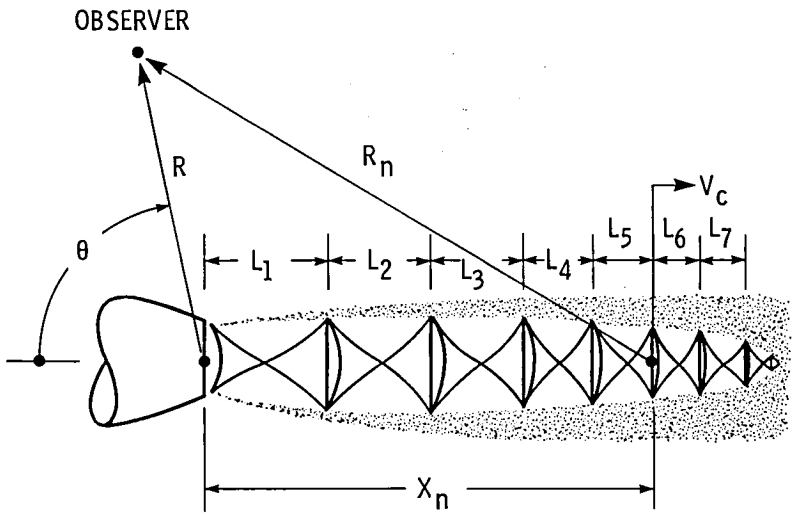

Figure 1. - Representation of a family of shock-cells.

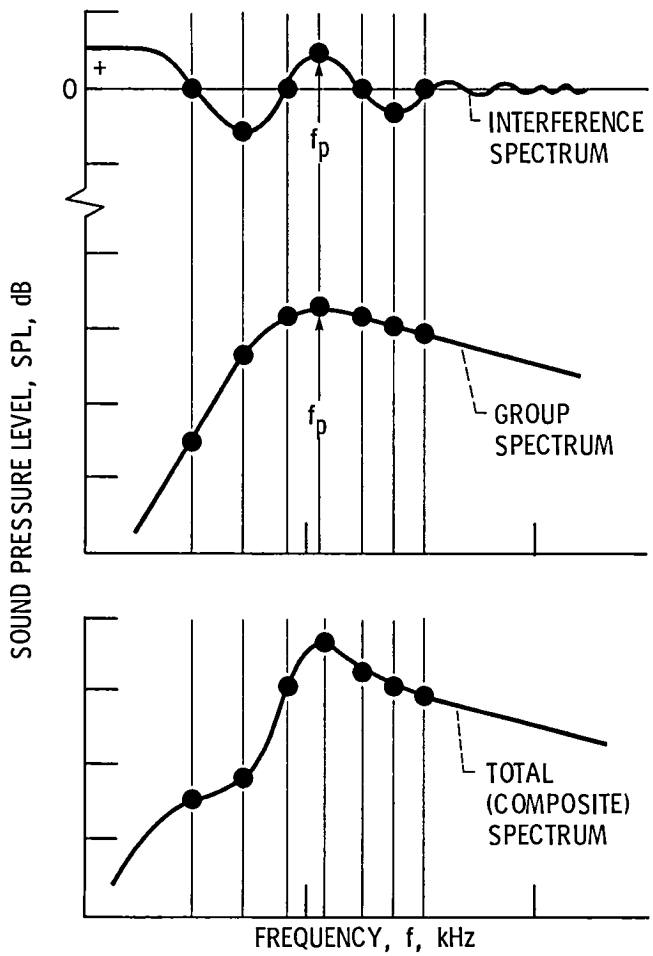

Figure 2. - Illustration of primary components of a convergent circular nozzle shock-cell noise spectrum.

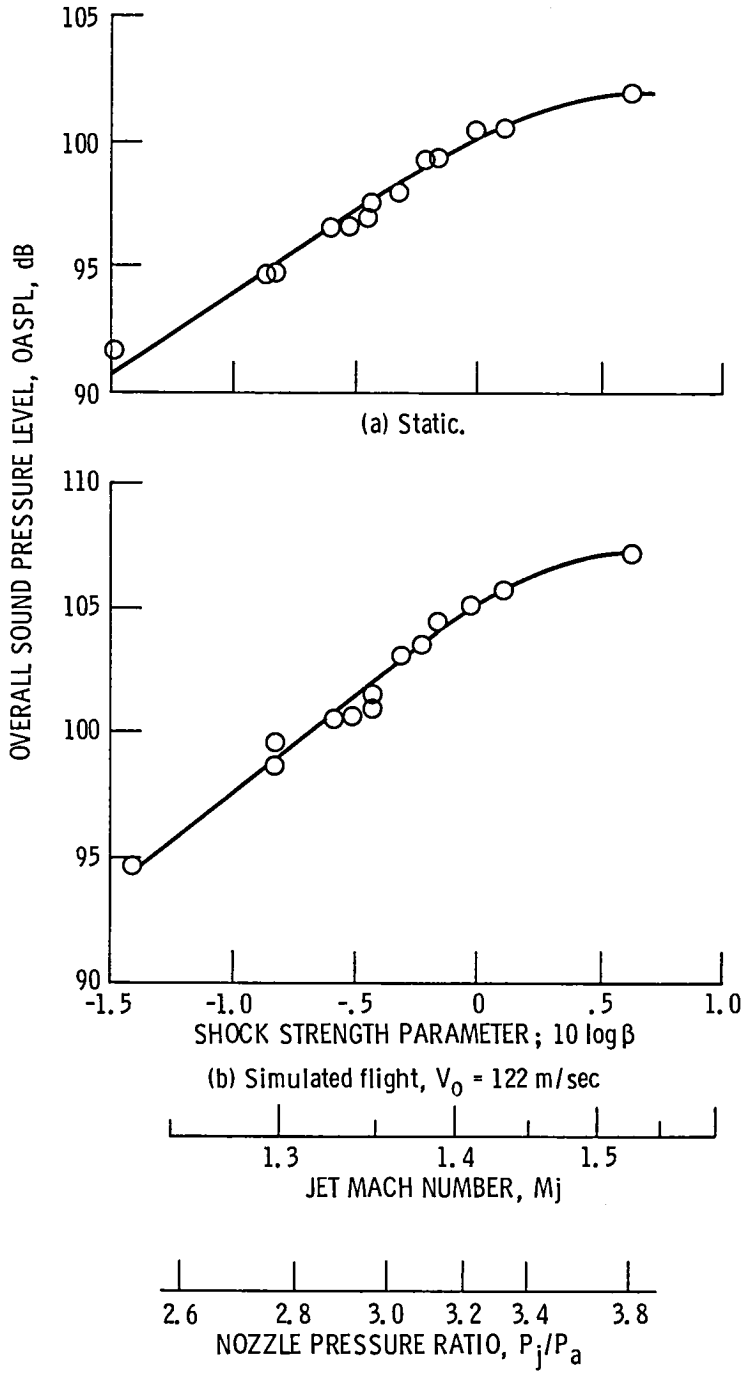

Figure 3. - Typical variation of shock noise OASPL in forward quadrant ($\theta = 50^0$) as function of β for convergent circular nozzle. Data scaled to 0.903-m^2 nozzle area and extrapolated to 730-m sideline; jet temperature $T_j \simeq 950$ K (ref. 8).

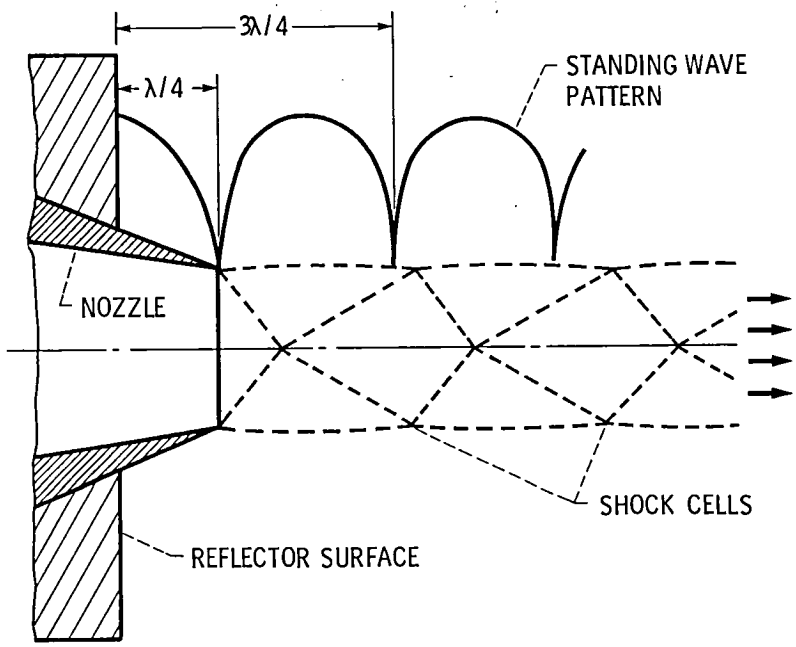

Figure 4. - Schematic diagram of nozzle exit and reflector showing the foam cancellation technique (ref. 6).

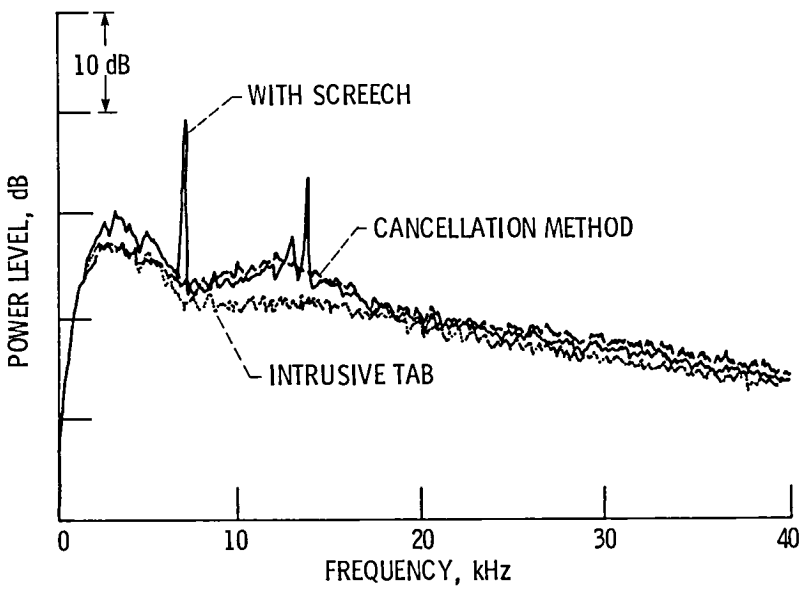

Figure 5. - Narrowband noise spectra from the reverberation room comparing screech cancellation to screech reduction with tab, $M_j = 1.4$ (ref. 6).

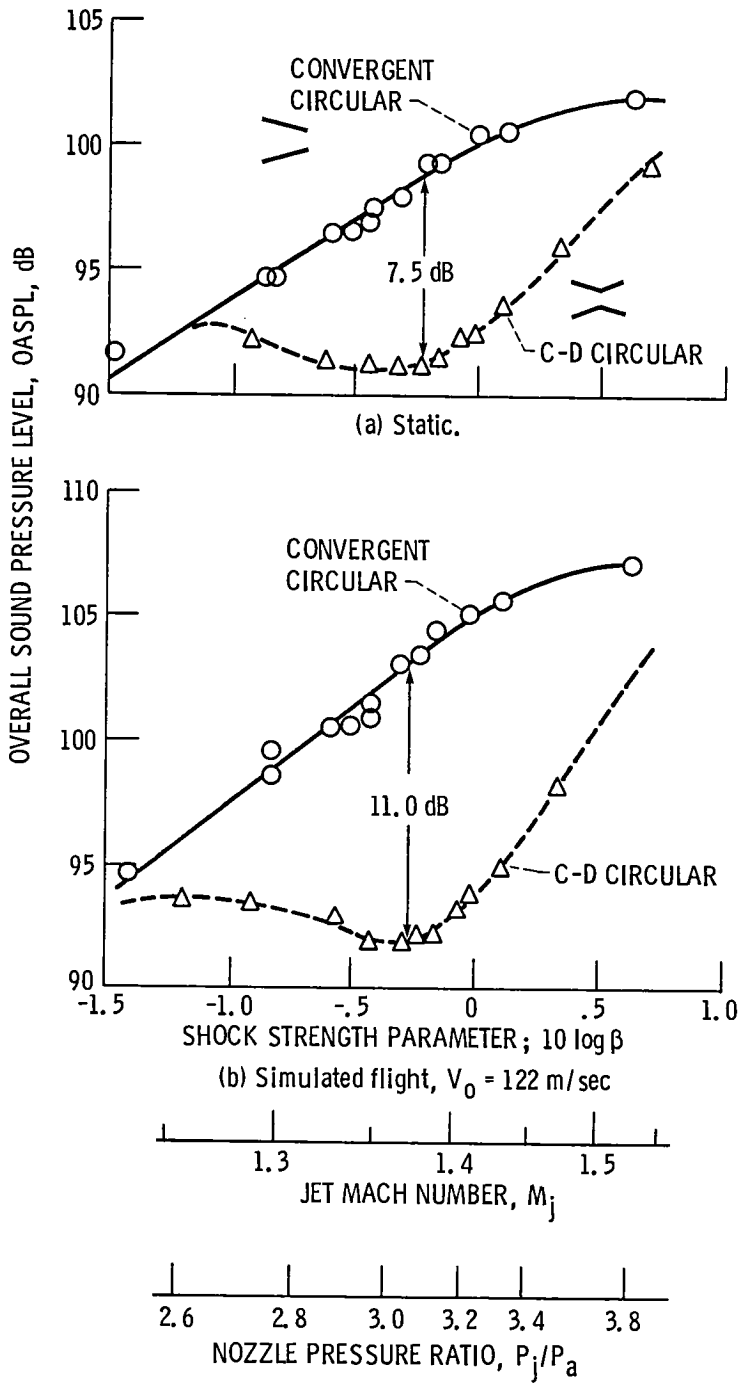

Figure 6. - Effectiveness of C-D termination in reducing circular nozzle shock noise OASPL in forward quadrant ($\theta = 50^0$); jet temperature, $T_j \cong 950$ K. Data scaled to 0.903-m^2 nozzle area and extrapolated to 730-m sideline (ref. 8).

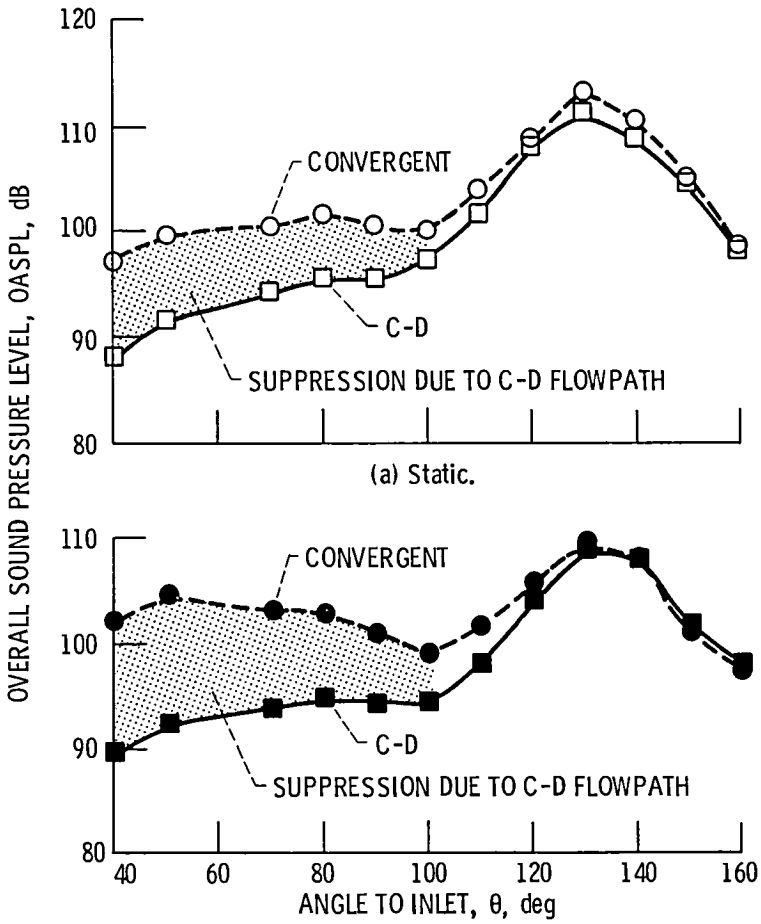

Figure 7. - Comparison of OASPL directivity of convergent and C-D nozzle at the C-D nozzle design conditions; jet temperature, T_j = 950 K. Data scaled to 0.903-m^2 nozzle area and extrapolated to 730-m sideline (ref. 8).

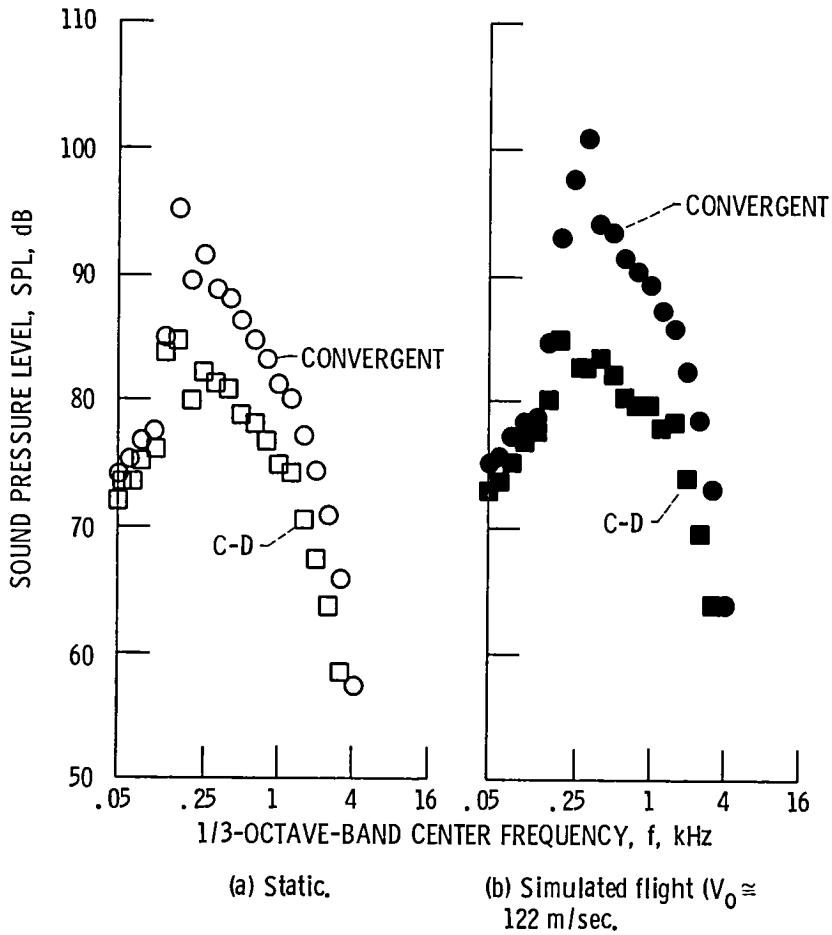

Figure 8. - Comparison of typical front quadrant ($\theta = 50^0$) spectra of convergent and C-D nozzles at the C-D nozzle design conditions; jet temperature, $T_j \cong 950$ K. Data scaled to 0.903-m^2 nozzle area and extrapolated to 730-m sideline (ref. 8).

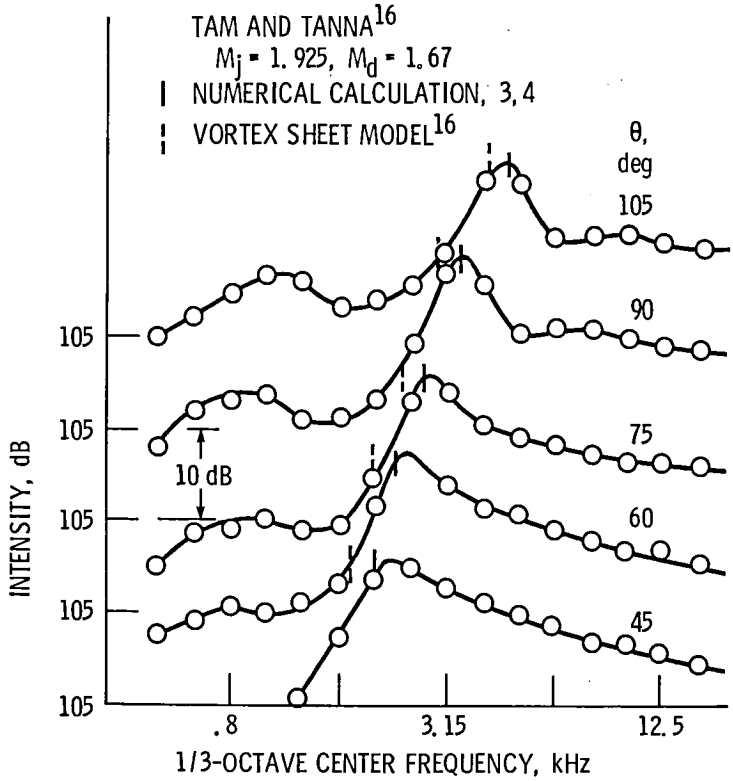

Figure 9. - Variation of shock associated noise peak frequency with angle.

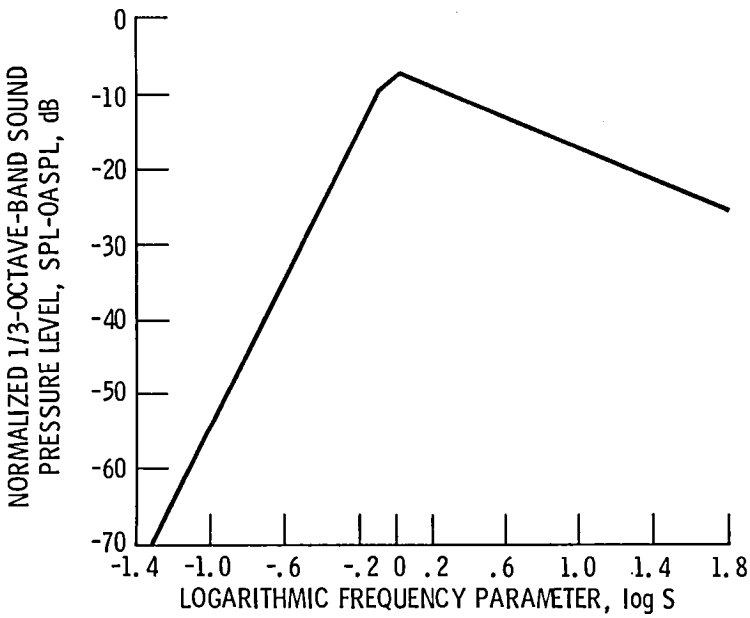

Figure 10. - Recommended 1/3-octave band spectrum for shock noise.

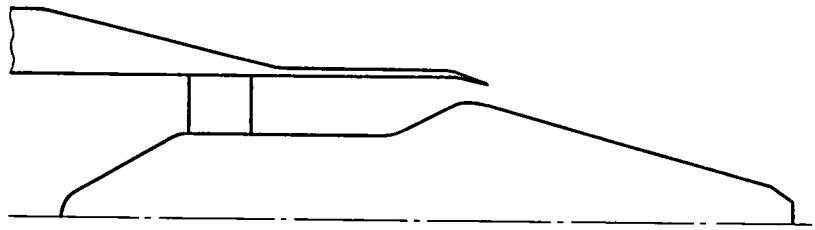

(a) Convergent termination.

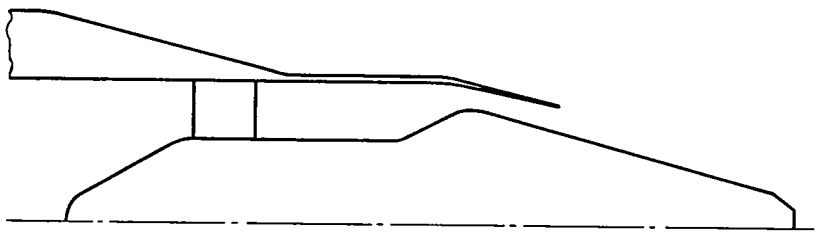

(b) Convergent-divergent (C-D) termination.

Figure 11. - Annular plug nozzle configurations.

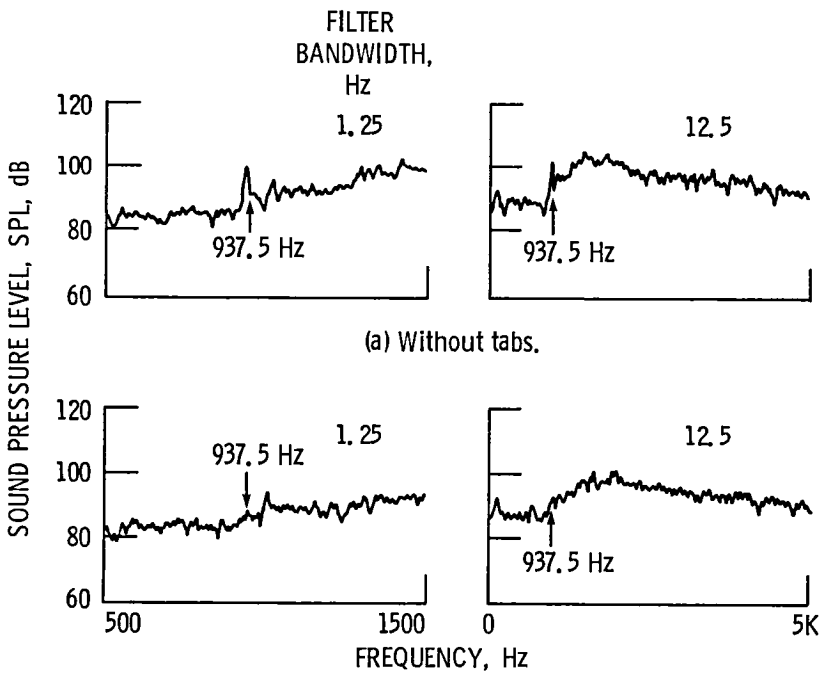

(b) With tabs.

Figure 12. - As-measured narrowband spectra at $\theta = 60^{0}$ for convergent annular plug nozzle with and without tabs; moderately heated jet, $T_j \cong 480$ K, at pressure ratio, $P_j/P_a \simeq 3.4$ (ref. 8).

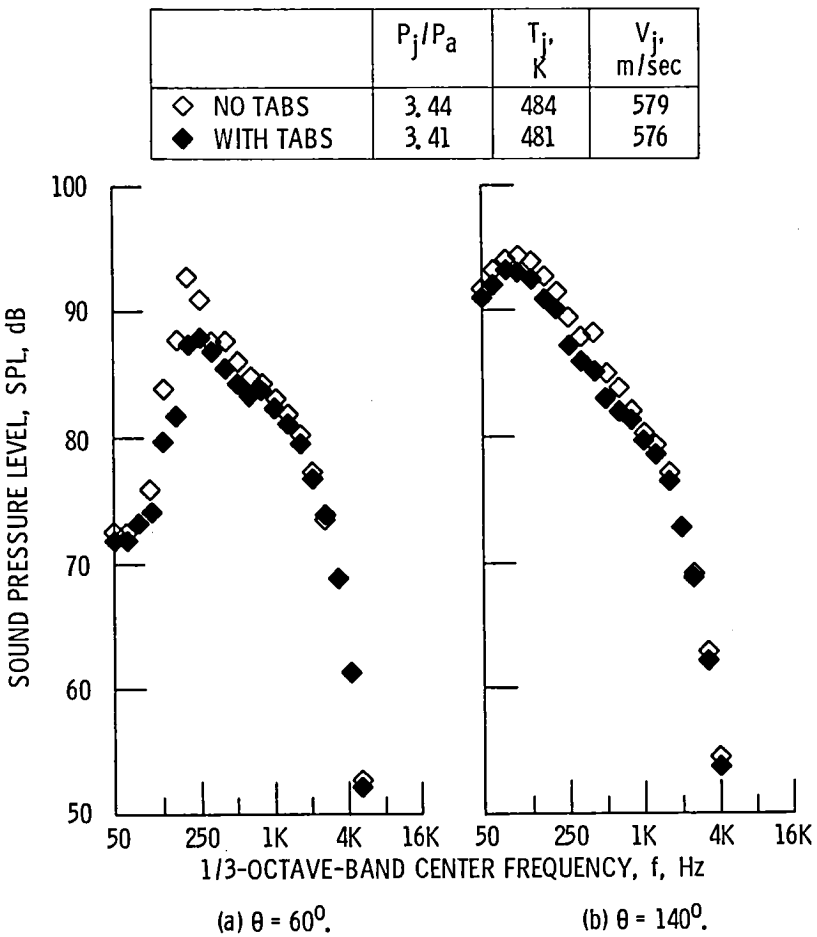

Figure 13. - Effects of screech tabs on SPL spectra: convergent annular plug nozzle (moderately heated jet). Static data scaled to 0.903-m^2 nozzle area and extrapolated to 730-m sideline (ref. 8).

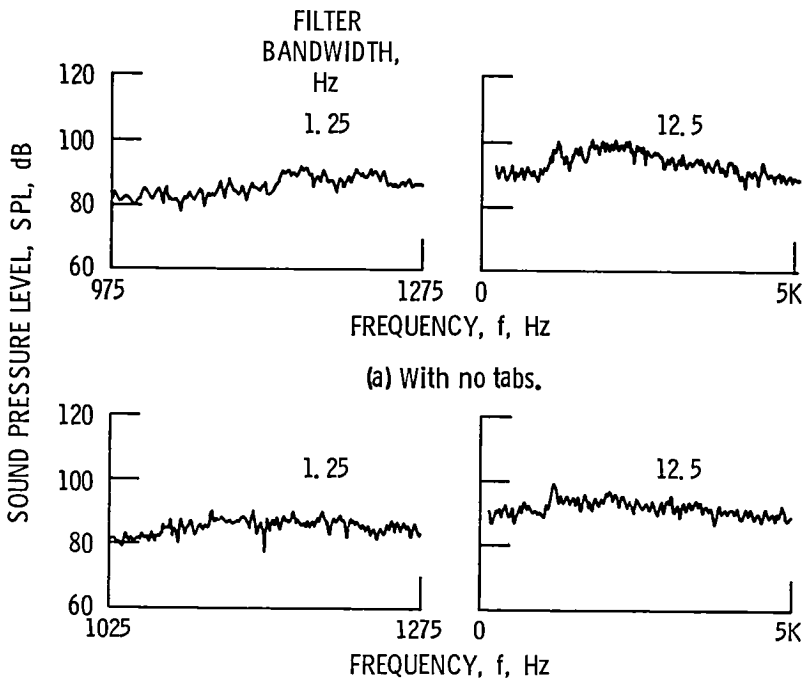

Figure 14. - As-measured narrowband SPL spectra at $\theta = 60^{0}$ for convergent annular plug nozzle with and without tabs; high temperature jet, $T_j \cong 960$ K, pressure ratio, $P_j/P_a = 3.34$ (ref. 8).

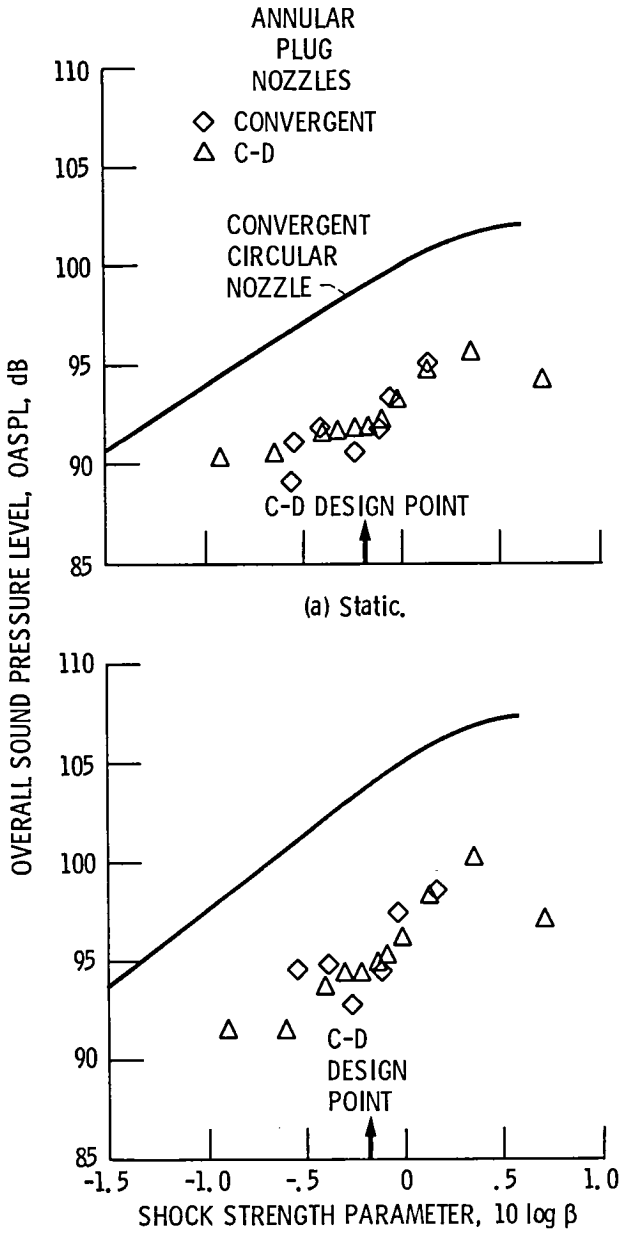

(a) Static.

(b) Simulated flight, V_0 = 122 m/sec

Figure 15. - Comparison of C-D annular plug nozzle OASPL with those of convergent annular plug nozzle and baseline convergent circular nozzle in forward quadrant, $\theta = 50^0$; jet temperature, $T_j \cong 960$ K. Data scaled to 0.903-m^2 nozzle area and extrapolated to 730-m sideline (ref. 9).

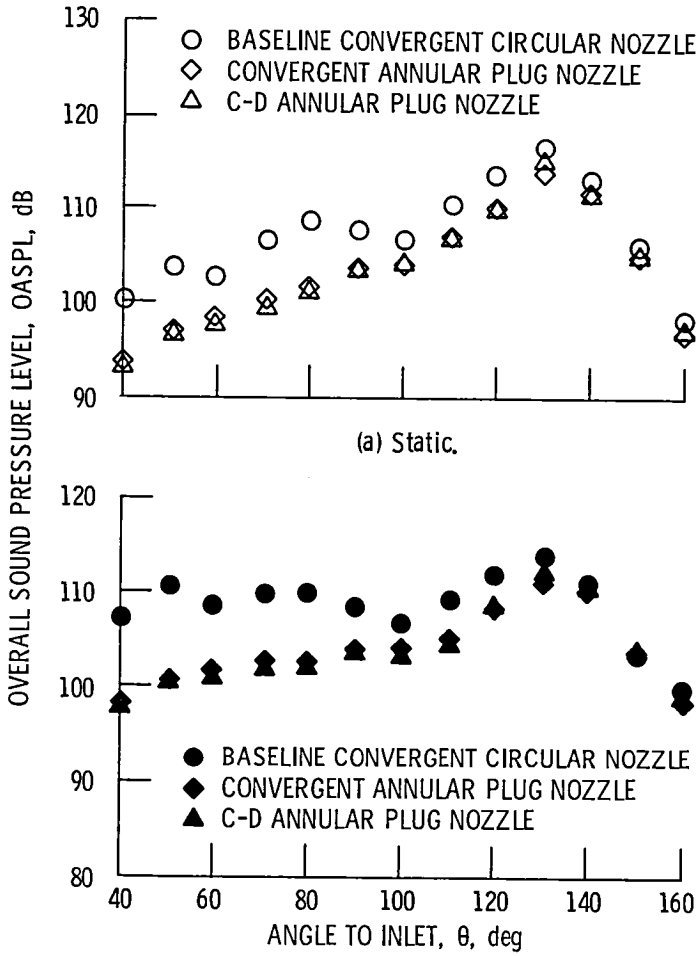

Figure 16. - Comparison of directivity of C-D annular plug nozzle with those of convergent annular plug nozzle and baseline convergent circular nozzle at C-D design conditions, $T_j \cong 960$ K. Data scaled to 0.903-m^2 nozzle area and extrapolated to 730-m sideline (ref. 8).

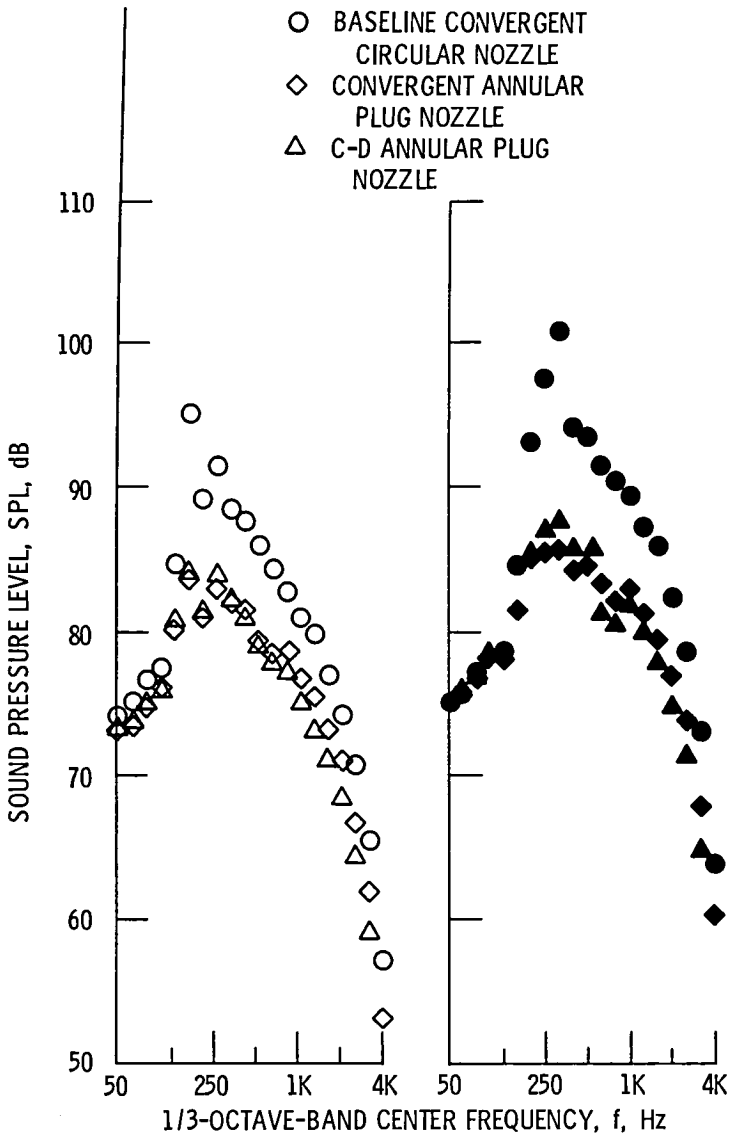

Figure 17. - Spectral comparison between C-D annular plug nozzle, convergent annular plug nozzle, and baseline convergent circular nozzle at C-D design conditions; forward quadrant angle, $\theta = 50^{o}$; jet temperature, $T_j \cong 960$ K. Data scaled to 0.903-m^2 nozzle area and extrapolated to 730-m sideline (ref. 8).

MODEL	P_j/P_a	T_j, K	D_e, cm	h, cm
CONVERGENT	3.16	967	14.4	2.06
CONVERGENT-DIVERGENT	3.12	962	14.4*	2.06*

*BASED ON THROAT AREA AND HEIGHT

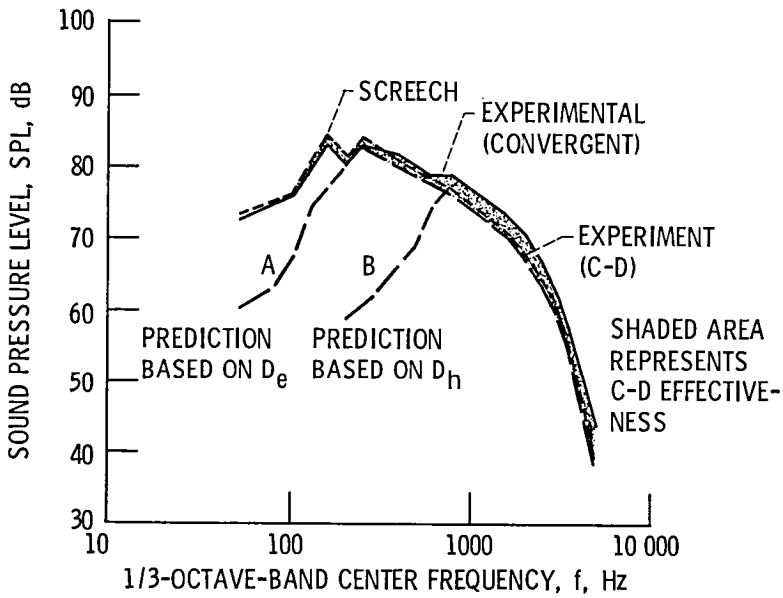

Figure 18. - Spectral comparison of shock-cell noise between modified predictions and both convergent and C-D data, illustrating spectral contribution of shocks formed on the plug and downstream of the plug; $\theta = 50^0$; static data scaled to 0.903-m^2 nozzle diameter and extrapolated to 730-m sideline (ref. 8). Lines A and B are not real predictions, but an illustration of prediction concept.

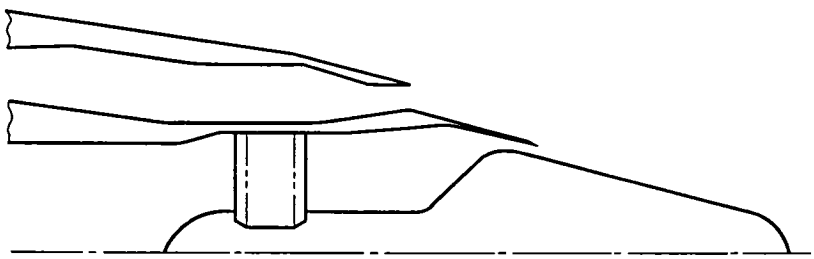

(a) Inner and outer nozzle terminations convergent, with truncated plug.

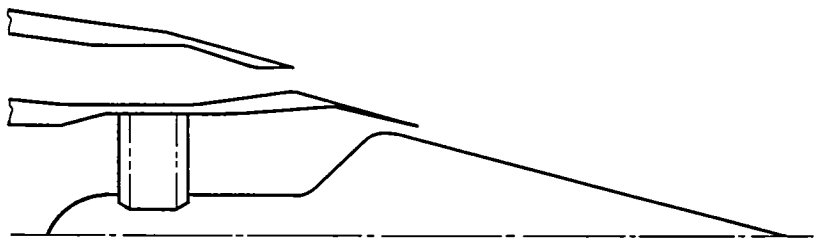

(b) Inner and outer nozzle terminations convergent, with extended plug.

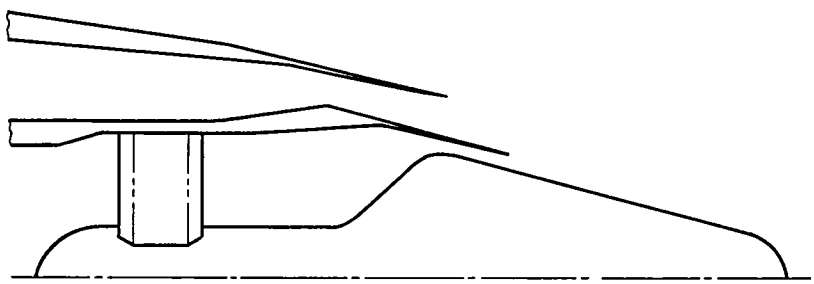

(c) Inner and outer nozzle terminations convergent-divergent, with truncated plug.

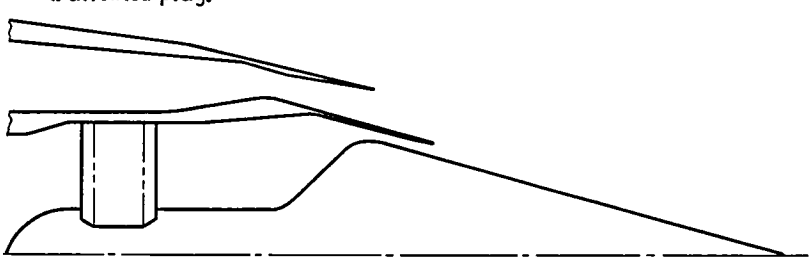

(d) Inner and outer nozzle terminations covergent-divergent, with extended plug.

Figure 19. - Coannular plug nozzle configurations (ref. 10).

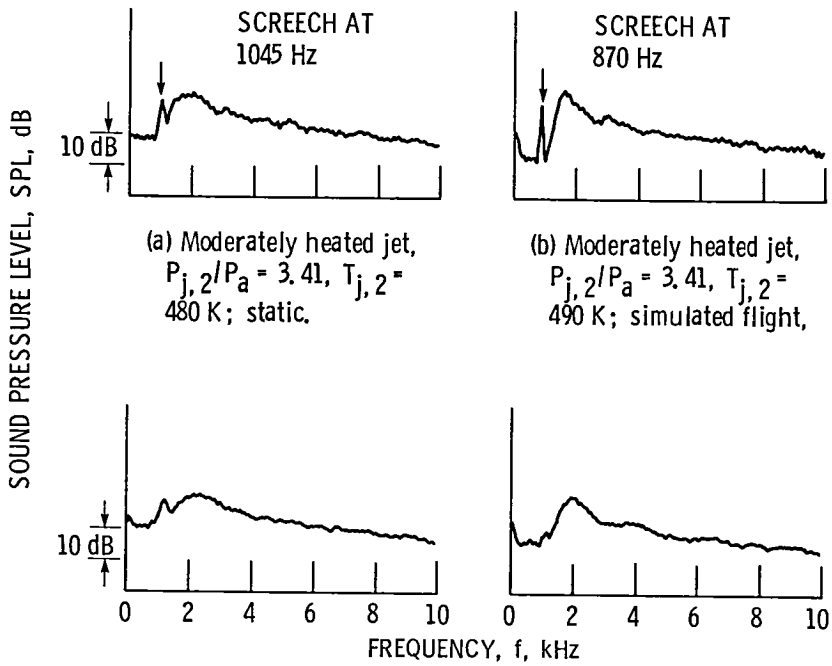

(a) Moderately heated jet, $P_{j,2}/P_a = 3.41$, $T_{j,2} = 480$ K; static.

(b) Moderately heated jet, $P_{j,2}/P_a = 3.41$, $T_{j,2} = 490$ K; simulated flight,

(c) High temperature jet, $P_{j,2}/P_a = 3.32$, $T_{j,2} = 940$ K; static.

(d) High temperature jet, $P_{j,2}/P_a = 3.33$, $T_{j,2} = 945$ K; simulated flight, $V_0 = 122$ m/sec.

Figure 20. - On-line narrowband data obtained with convergent coannular nozzle at two outer stream temperatures, with constant inner stream conditions, $P_{j,1}/P_a \cong 3.13$, $T_{j,1} \cong 480$ K.

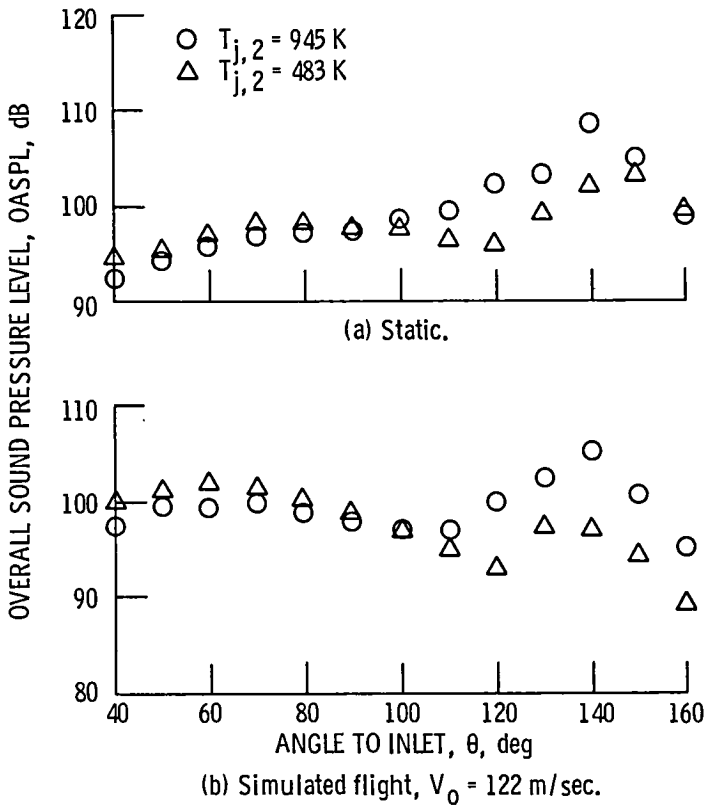

Figure 21. - Effect of outer stream temperature on OASPL-directivity of convergent coannular nozzle with truncated plug.

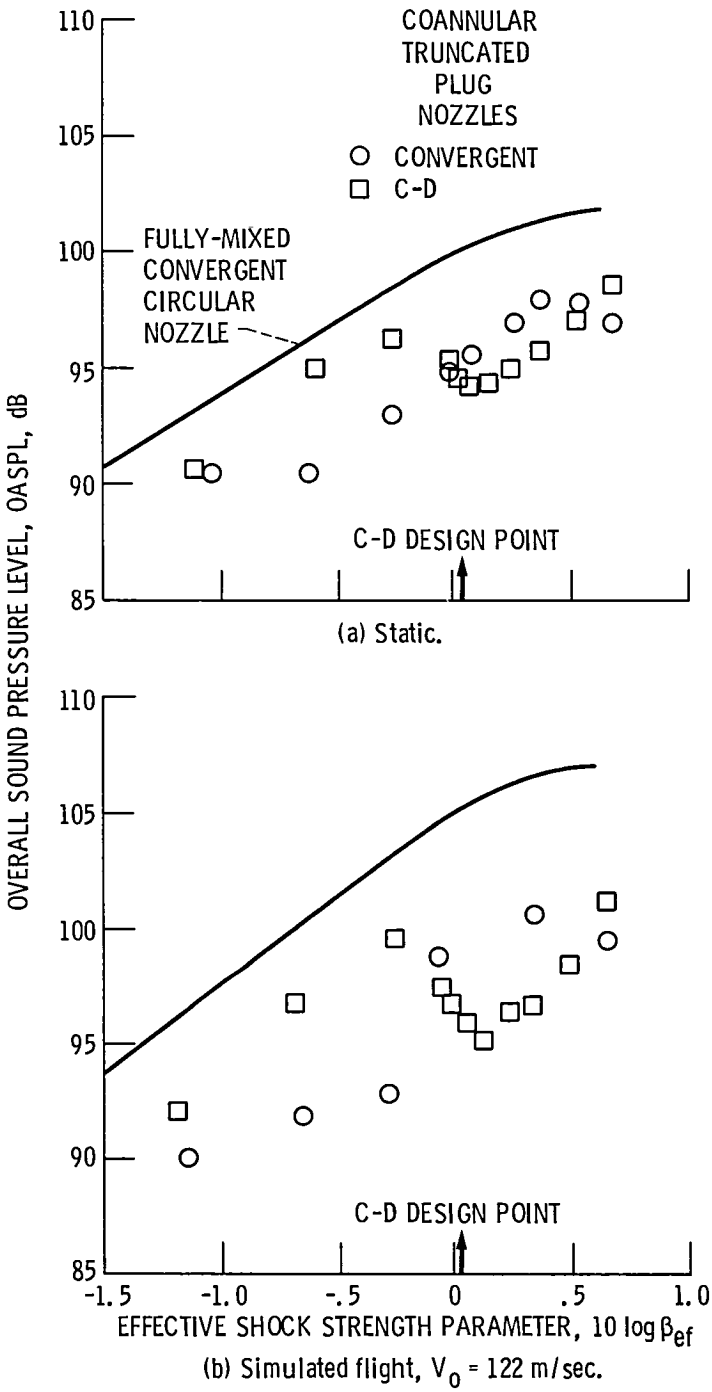

Figure 22. - Comparison of C-D coannular truncated-plug nozzle OASPL with those of convergent coannular truncated-plug nozzle and baseline fully-mixed convergent circular nozzle in forward quadrant, $\theta = 60^0$; inner-stream temperature, $T_{j,1} \simeq 480$ K; outer-stream temperature, $T_{j,2} \simeq 940$ K. Data scaled to 0.903-m^2 total nozzle area and extrapolated to a 730-m sideline (ref. 11).

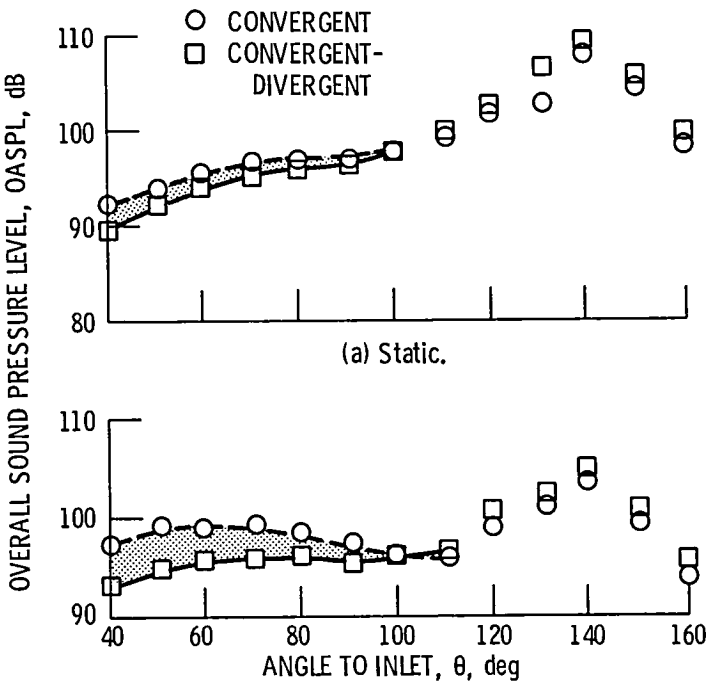

Figure 23. - Effect of C-D terminations on coannular nozzle directivity at C-D design point; $T_{j,1} \cong 485$ K, $T_{j,2} \cong 940$ K. Data scaled to 0.903-m^2 total nozzle area and extrapolated to 730 m sideline (ref. 10).

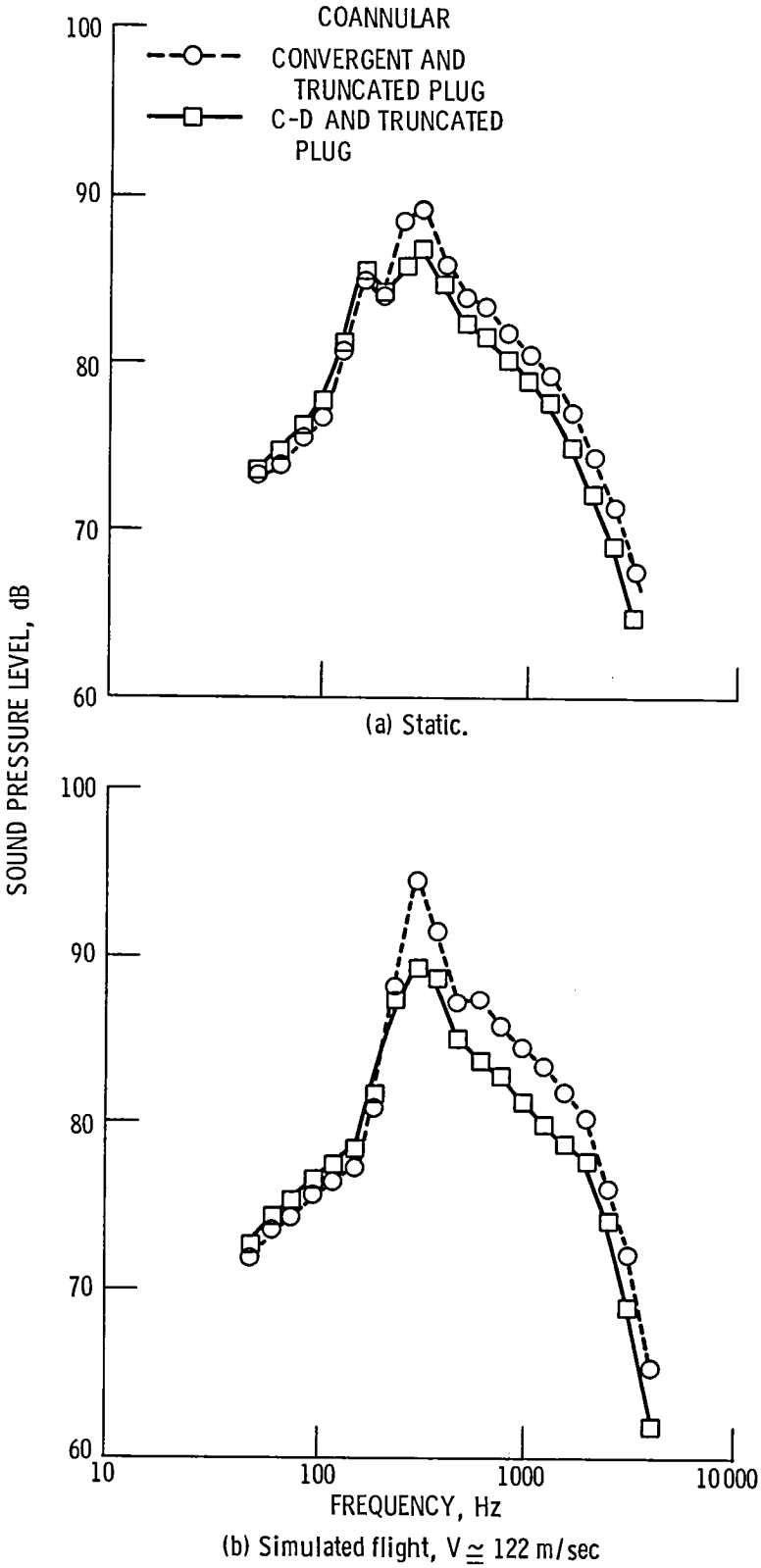

Figure 24. - Effect of C-D termination on forward quadrant spectra ($\theta = 60^{0}$) for coannular nozzle at C-D design point; $T_{j,1} \cong 480$ K, $T_{j,2} \cong 940$ K. Data scaled to 0.903-m^2 total nozzle area and extrapolated to 730-m sideline (ref. 10).

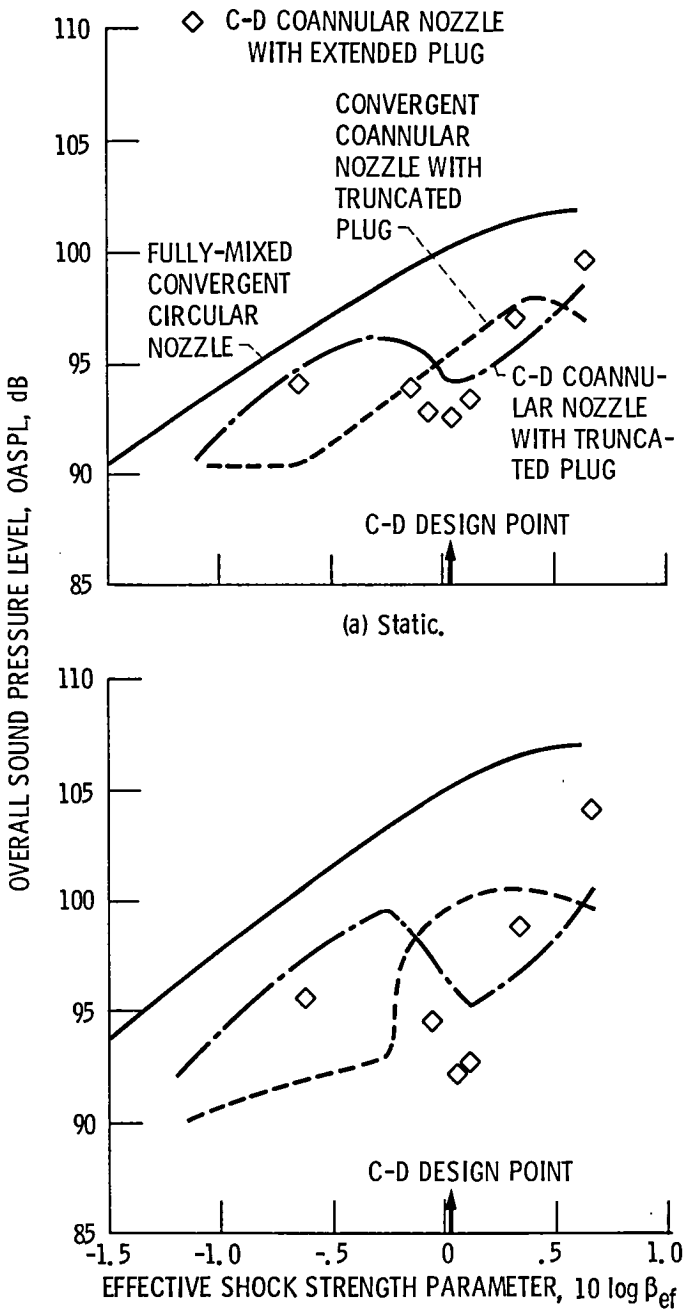

Figure 25. - Effectiveness of extended plug termination in reducing coannular nozzle OASPL in the forward quadrant, $\theta = 60^{o}$; inner-stream temperature, $T_{j,1} \cong 480$ K; outer-stream temperature, $T_{j,2} \cong 940$ K. Data scaled to 0.903-m^2 total nozzle area and extrapolated to a 730-m sideline (ref. 11).

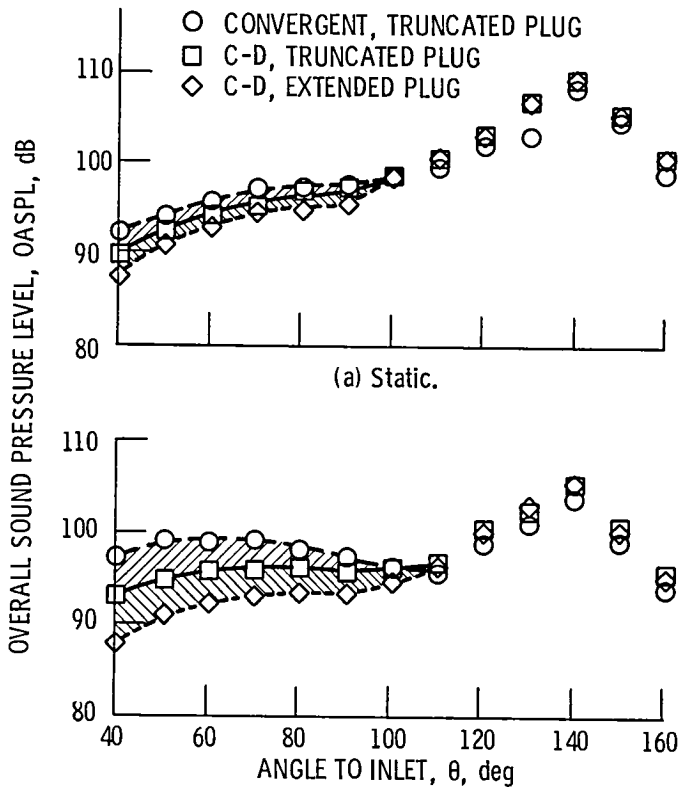

(a) Static.

(b) Simulated flight, $V_0 \approx 122$ m/sec.

Figure 26. - Effect of plug tip geometry C-D coannular nozzle directivity at C-D design conditions; $T_{j,1} \approx 480$ K, $T_{j,2} \approx 940$ K. Data scaled to 0.903-m^2 total nozzle area and extrapolated to 730-m sideline (ref. 10).

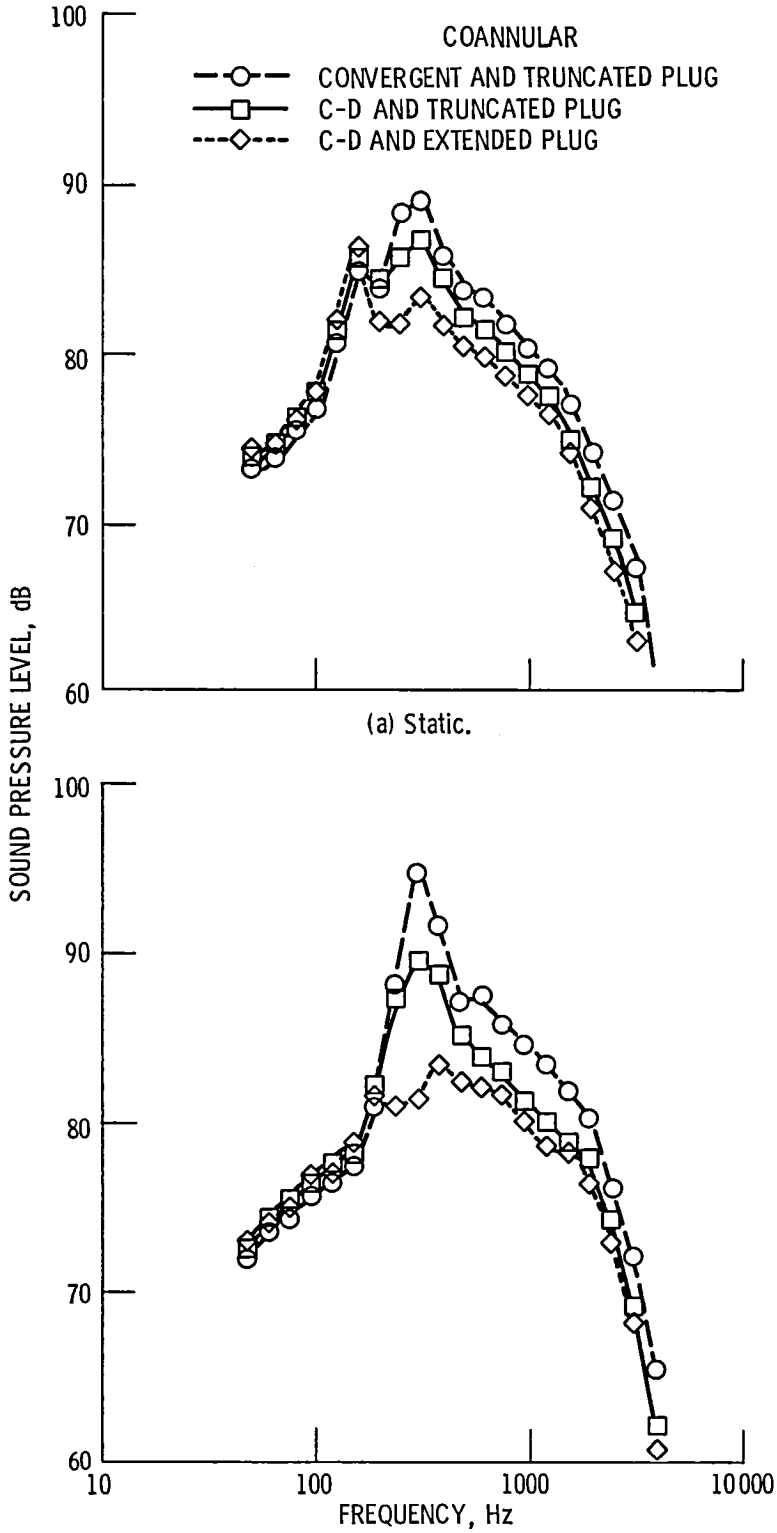

(a) Static.

(b) Simulated flight, $V_0 \cong 122$ m/sec

Figure 27. - Effect of plug tip geometry on forward quadrant spectra ($\theta = 60^0$) for C-D coannular nozzle at design point; $T_{j,1} \simeq 480$ K, $T_{j,2} \simeq 940$ K. Data scaled to 0.903 m^2 total nozzle area and extrapolated to 730-m sideline (ref. 10).

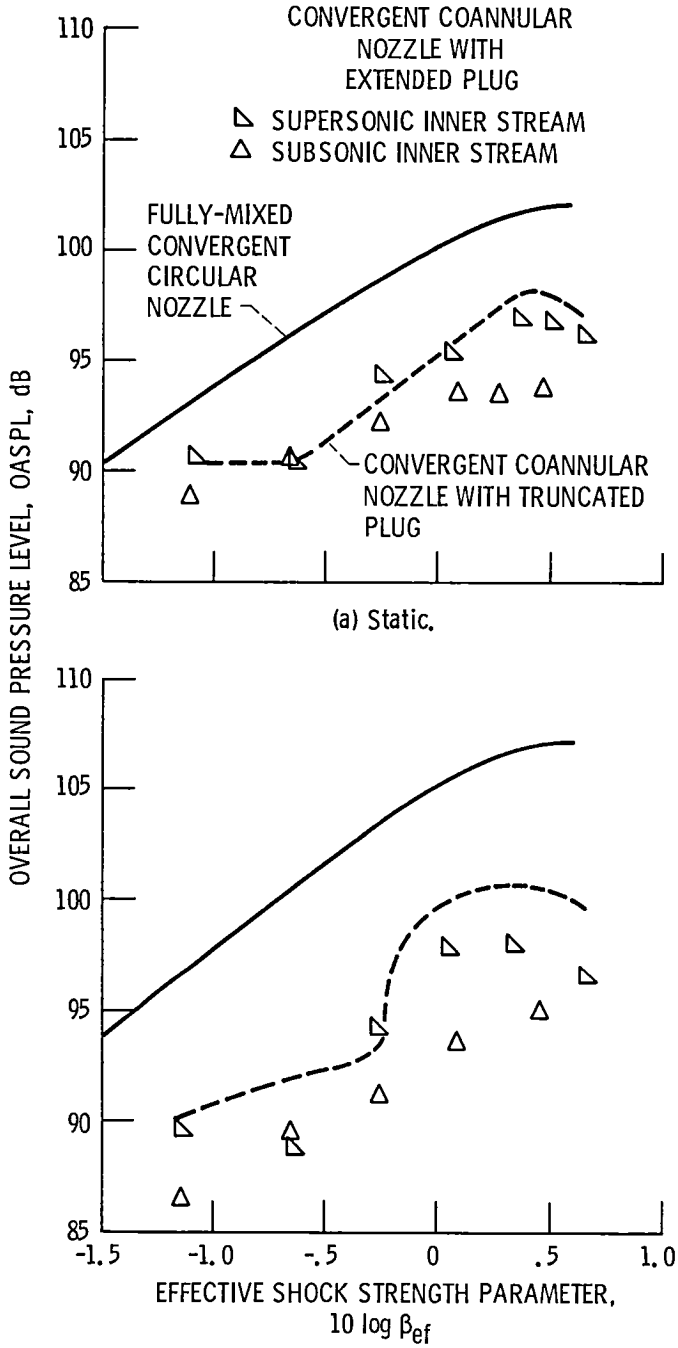

Figure 28. - Effectiveness of subsonic inner stream conditions in reducing OASPL for convergent coannular nozzle in the forward quadrant, $\theta = 60^{o}$; outer-stream temperature, $T_{j,2} \cong 940$ K. Data scaled to 0.903-m^2 total nozzle area and extrapolated to a 730-m sideline (ref. 11).

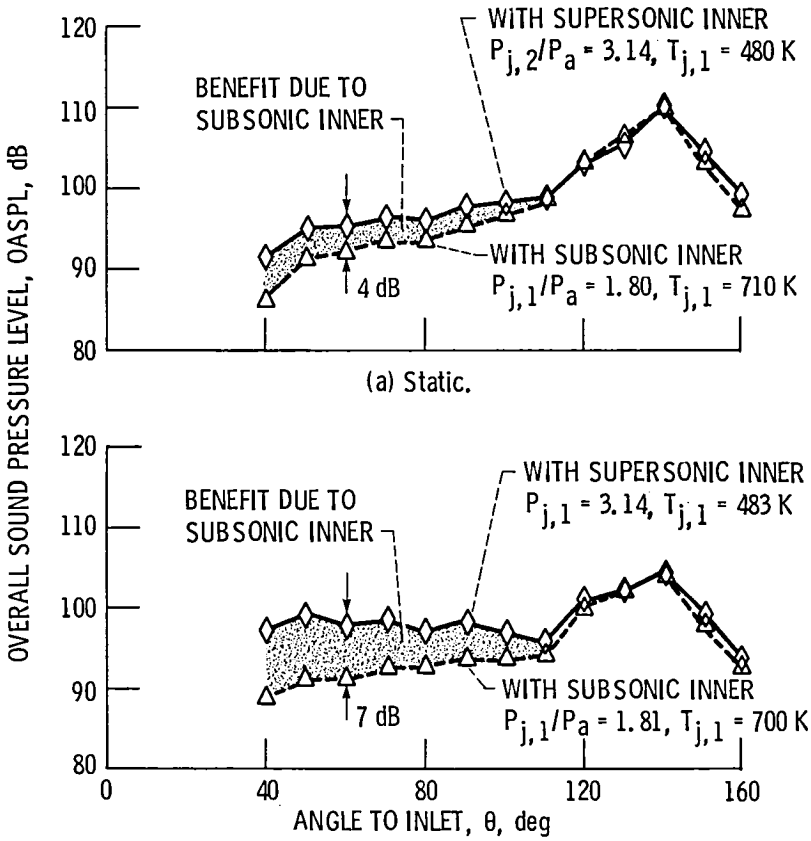

Figure 29. - Typical static and simulated flight OASPL-directivities of convergent coannular nozzle with extended plug for subsonic and supersonic inner streams for a given underexpanded outer stream; $P_{j,2}/P_a \cong 3.32$, $T_{j,2} \cong 940$ K.

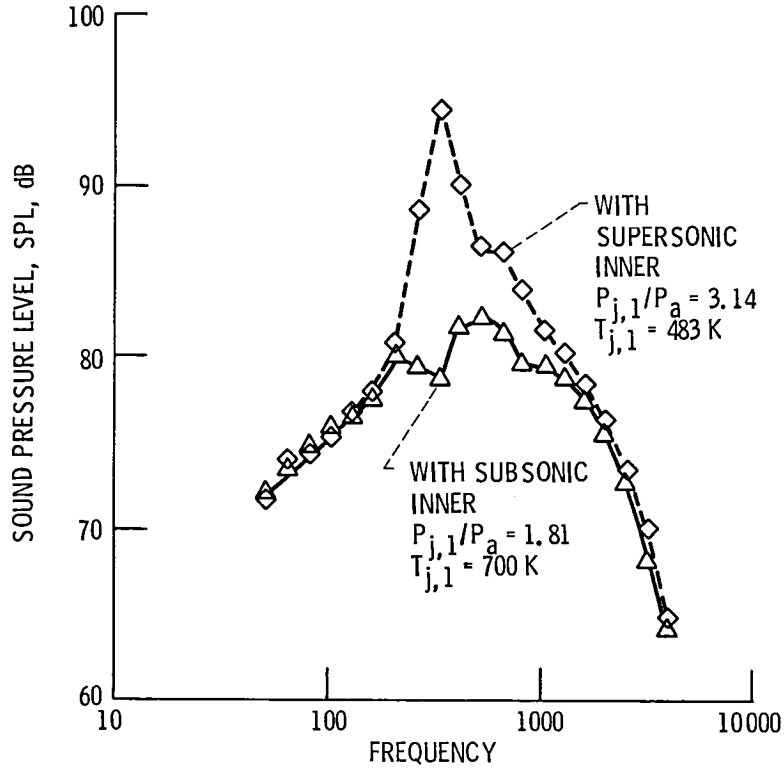

Figure 30. - Typical simulated flight front quadrant spectra at $\theta = 60^0$ for convergent coannular nozzle with extended plug for subsonic and supersonic inner streams for a given underexpanded outer stream; $P_{j,2}/P_a \cong 3.32$; $T_{j,2} \cong 900$ K.

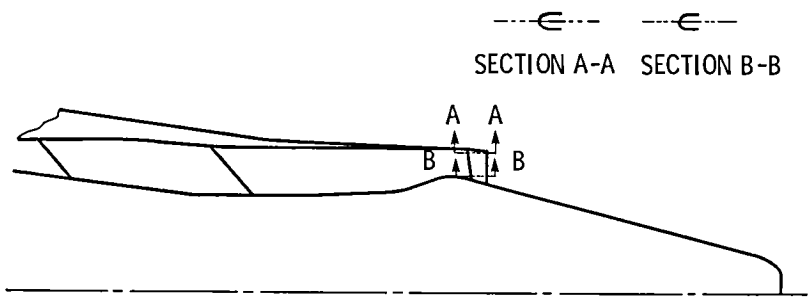

(a) Convergent flow element terminations.

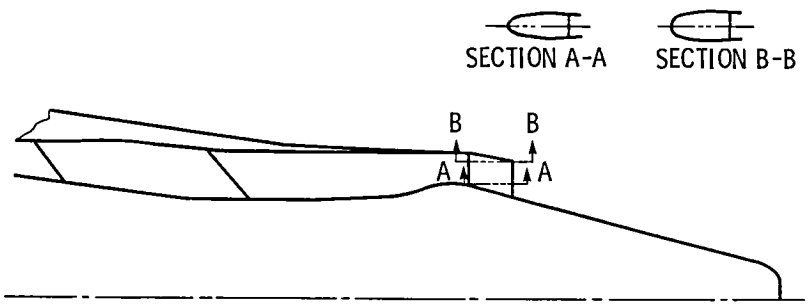

(b) C-D flow element terminations.

Figure 31. - 20 chute annular plug suppressor configurations (ref. 8).

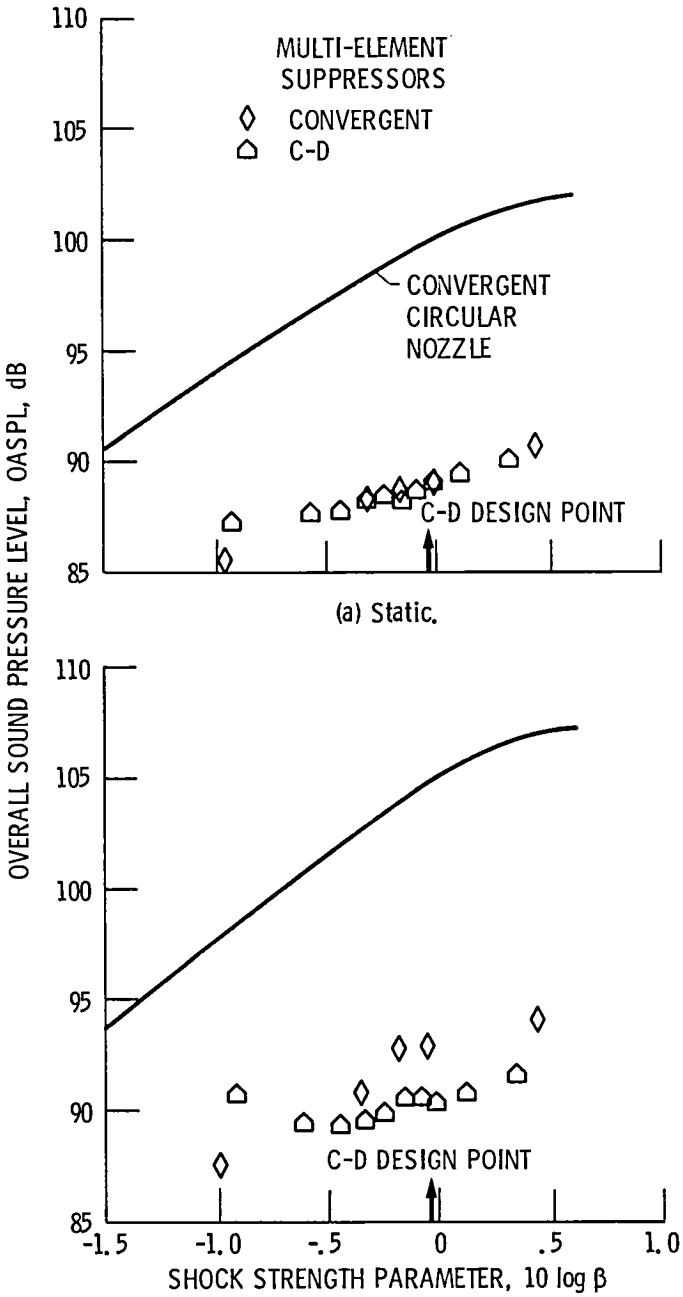

(a) Static.

(b) Simulated flight, V_0 = 122 m/sec.

Figure 32. - Comparison of C-D multi-element suppressor nozzle OASPL with those of convergent multi-element suppressor and baseline convergent circular nozzle in forward quadrant, $\theta = 50^0$; jet temperature, $T_j \simeq 950$ K. Data scaled to 0.903-m^2 nozzle area and extrapolated to 730-m sideline (ref. 9).

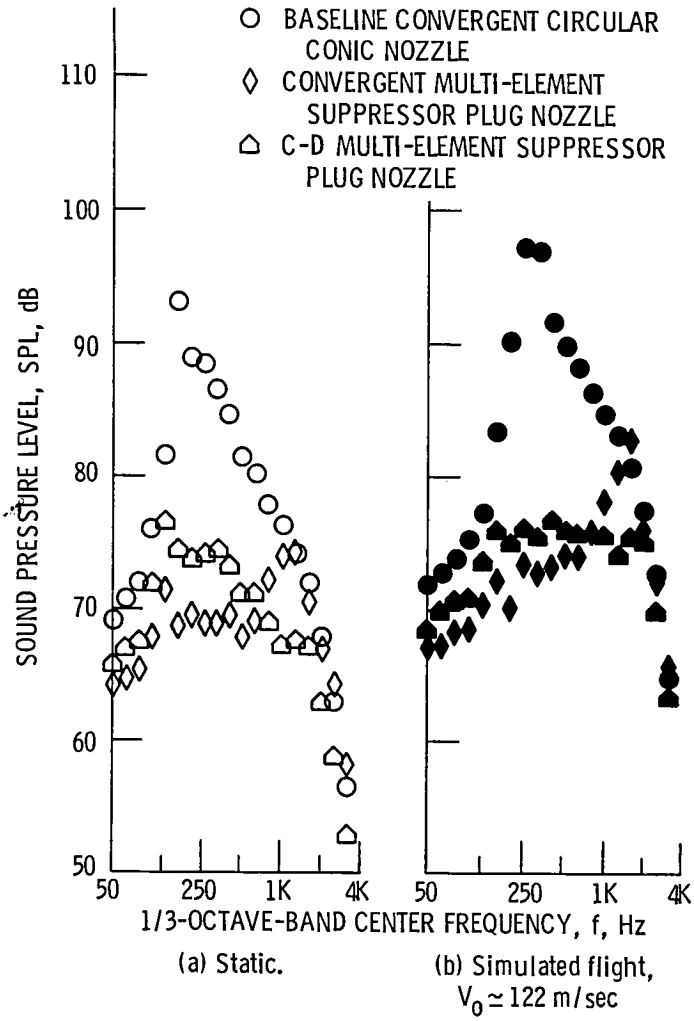

Figure 33. - Spectral comparison between baseline convergent circular nozzle, convergent multi-element suppressor plug nozzle, and C-D multi-element suppressor plug nozzle, $\theta = 50^0$; $T_j \cong$ 960 K. Data scaled to 0.903 m^2 nozzle area and extrapolated to 730-m sideline (ref. 8).

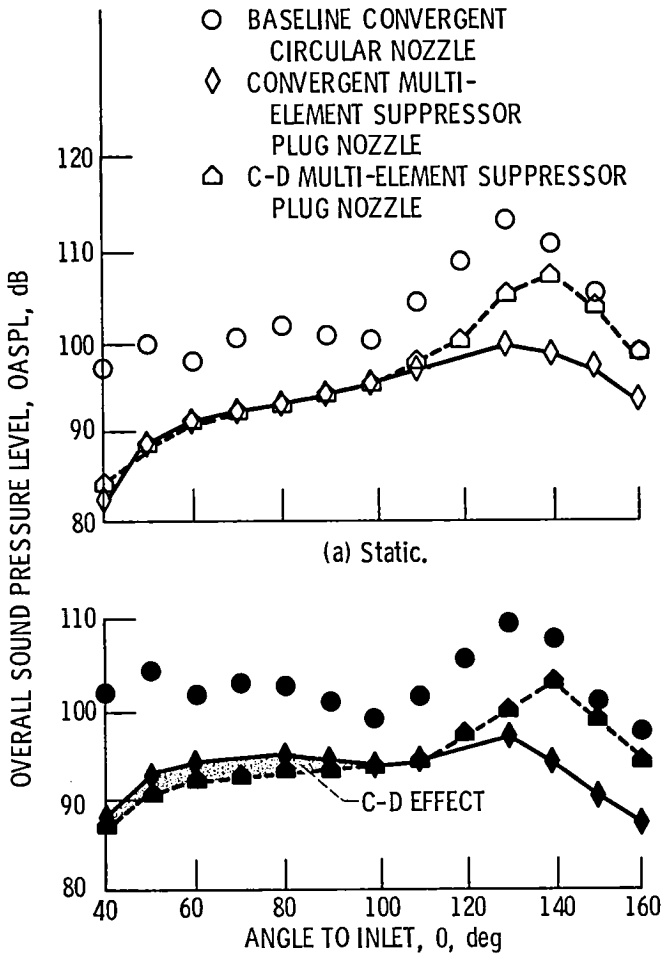

Figure 34 - OASPL directivity comparisons between baseline convergent circular nozzle, convergent multi-element suppressor plug nozzle, and C-D multi-element suppressor plug nozzle, $T_j \simeq 960$ K. Data scaled to 0.903-m^2 nozzle area and extrapolated to 730-m sideline (ref. 8).

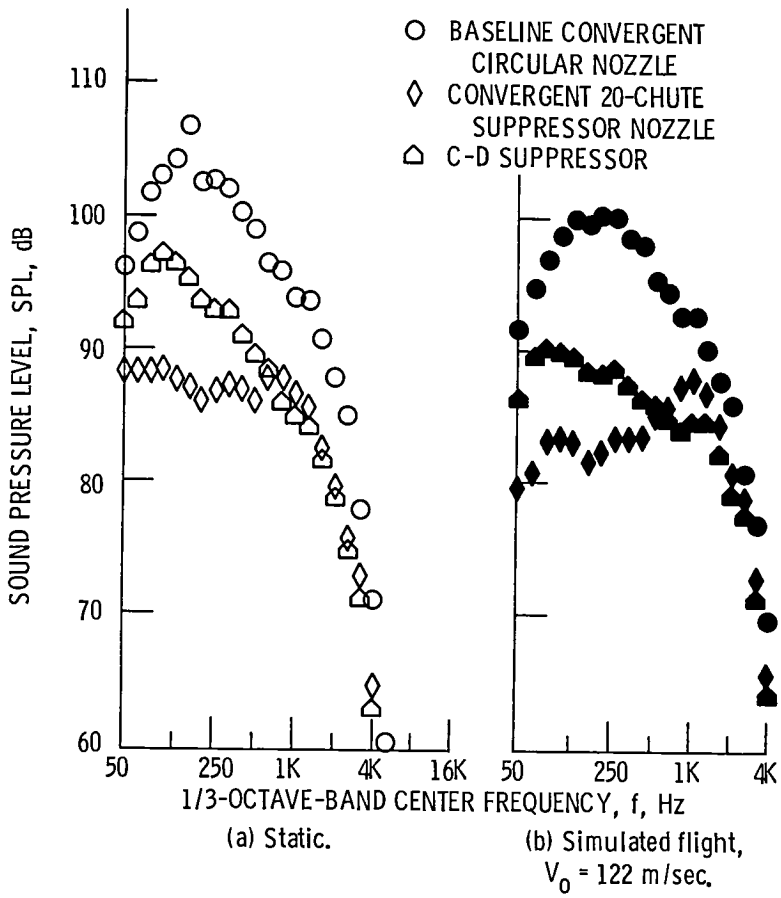

Figure 35. - Spectral comparison between convergent circular nozzle, convergent multi-element suppressor plug nozzle, and C-D multi-element suppressor plug nozzle, $\theta = 140^{o}$, $T_j \simeq 960$ K. Data scaled to 0.903-m^2 nozzle area and extrapolated to 730-m sideline.

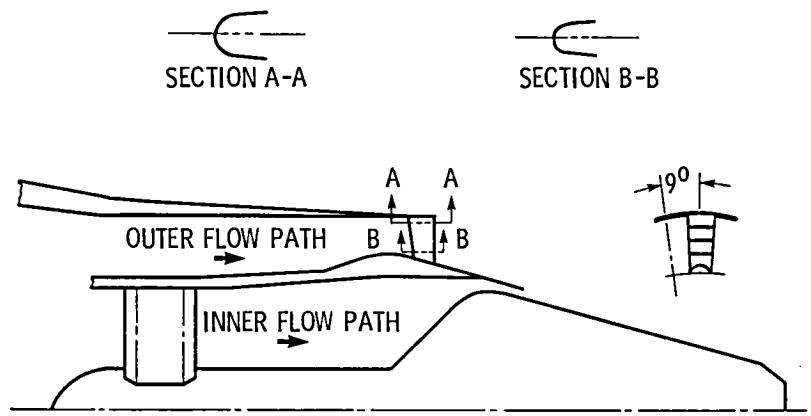

(a) Convergent flow element terminations.

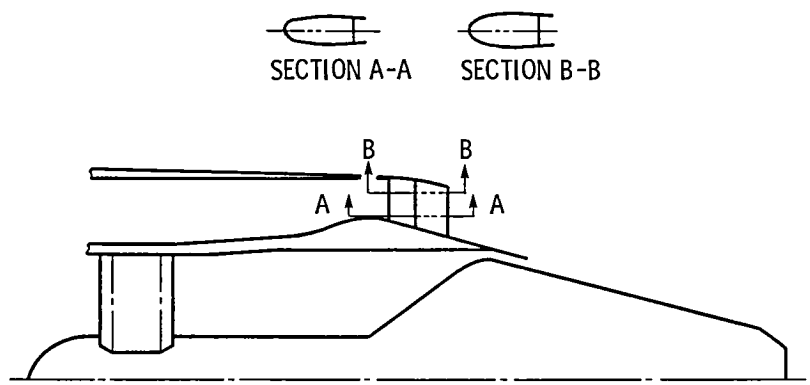

(b) C-D flow element termination.

Figure 36. - 20-chute outer stream suppressor configurations (ref. 10).

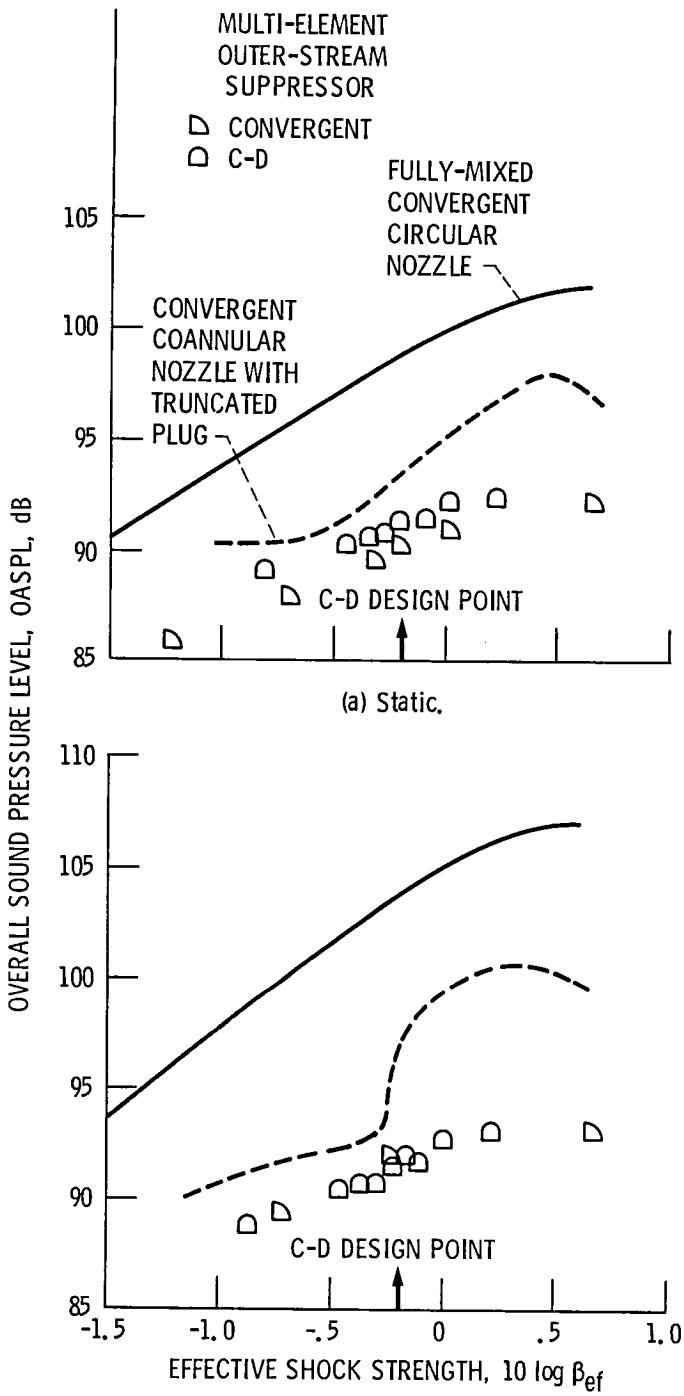

(a) Static.

(b) Simulated flight, $V_0 \cong 122$ m/sec.

Figure 37. - Effectiveness of C-D nozzle terminations on OASPL in forward quadrant, $\theta = 60^0$, for dual-stream nozzle with multi-element outer-stream suppressor; inner-stream temperature, $T_{j,2} \cong 940$ K. Data scaled to 0.903-m^2 total nozzle area and extrapolated to 730-m sideline (ref. 11).

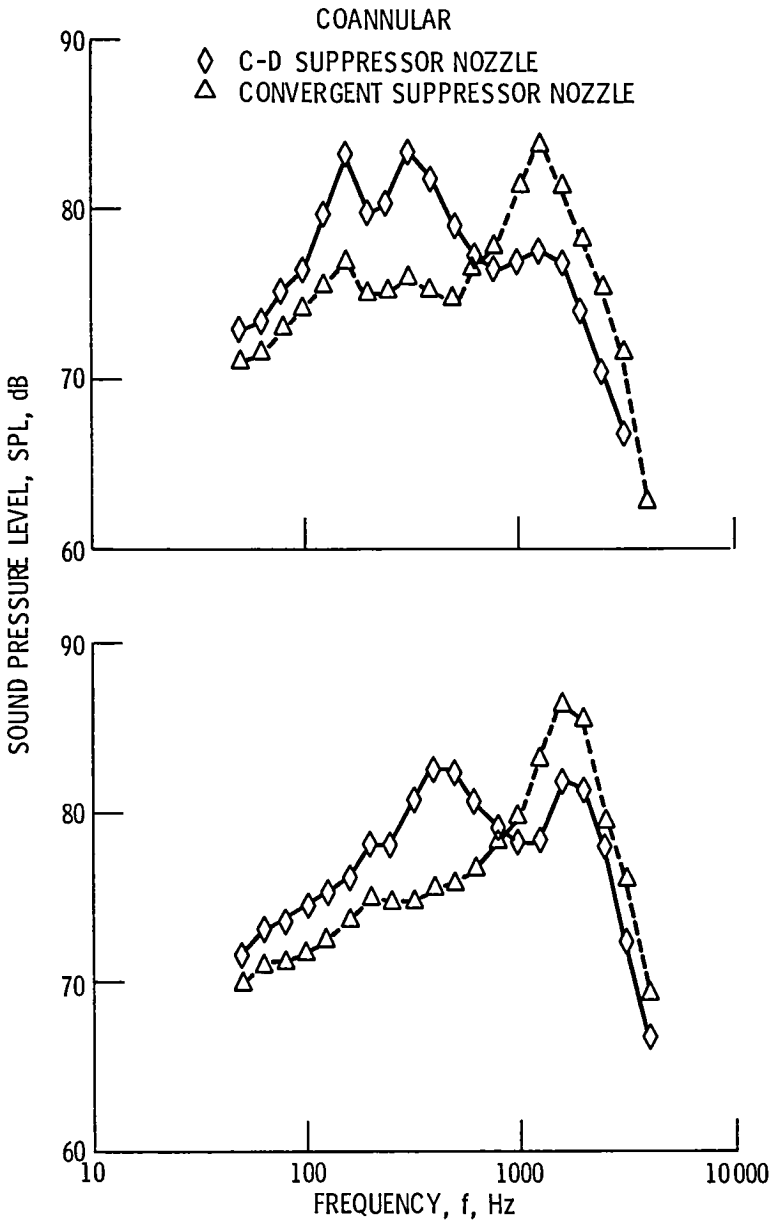

(b) Simulated flight, $V \approx 122$ m/sec.

Figure 38. - Typical static and simulated flight front quadrant spectral comparison at $\theta = 60^0$ between coannular C-D and convergent suppressor nozzles at C-D design conditions; $P_{j,1}/P_a \cong 2.91$; $P_{j,2}/P_a \cong 3.14$; $T_{j,1} \cong 480$ K; $T_{j,2} \cong 950$ K. Data scaled up to total nozzle area of 0.903 m^2 and extrapolated to 730 m sideline.

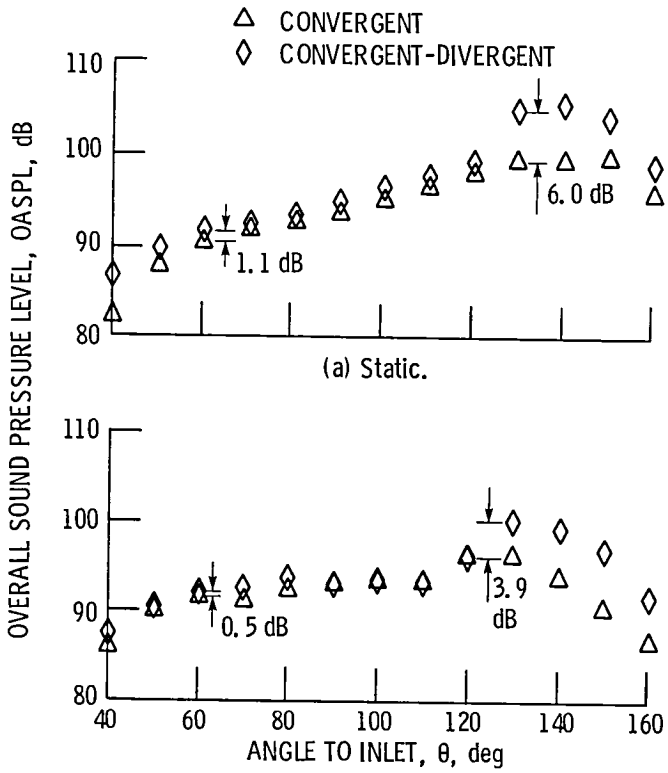

Figure 39. - Comparison of OASPL-directivities of coannular suppressor C-D nozzle with those of coannular suppressor convergent nozzle at C-D design conditions; inner-stream temperature, $T_{j,1} \cong 450$ K; outer-stream temperature, $T_{j,2} \cong 950$ K. Data scaled to 0.903-m^2 total nozzle area and extrapolated to 730-m sideline (ref. 10).

1. Report No.	2. Government Accession No.	3. Recipient's Catalog No.
NASA TM-83799		

4. Title and Subtitle	5. Report Date
Supersonic Jet Shock Noise Reduction	6. Performing Organization Code: 505-31-3B

7. Author(s)	8. Performing Organization Report No.
James R. Stone	E-2299
	10. Work Unit No.

9. Performing Organization Name and Address	11. Contract or Grant No.
National Aeronautics and Space Administration Lewis Research Center Cleveland, Ohio 44135	
	13. Type of Report and Period Covered: Technical Memorandum
12. Sponsoring Agency Name and Address	14. Sponsoring Agency Code
National Aeronautics and Space Administration Washington, D.C. 20546	

15. Supplementary Notes

Prepared for the Ninth Aeroacoustics Conference sponsored by the American Institute of Aeronautics and Astronautics, Williamsburg, Virginia, October 15-17, 1984.

16. Abstract

Shock-cell noise has been identified as a potentially significant problem for advanced supersonic aircraft at takeoff. Therefore NASA has conducted fundamental studies of the phenomena involved and model-scale experiments aimed at developing means of noise reduction. This paper reviews the results of a series of studies conducted to determine means by which supersonic jet shock noise can be reduced to acceptable levels for advanced supersonic cruise aircraft. Theoretical studies were conducted on the shock associated noise of supersonic jets from convergent-divergent (C-D) nozzles. Laboratory studies were conducted on the influence of narrowband shock screech on broadband noise and on means of screech reduction. The usefulness of C-D nozzle passages was investigated at model scale for single-stream and dual-stream nozzles. The effect of off-design pressure ratio was determined under static and simulated flight conditions for jet temperatures up to 960 K. Annular and coannular flow passages with center plugs and multielement suppressor nozzles were evaluated, and the effect of plug tip geometry was established. In addition to the far-field acoustic data, mean and turbulent velocity distributions were obtained with a laser velocimeter, and shadowgraph images of the flow field were obtained.

17. Key Words (Suggested by Author(s))	18. Distribution Statement
Noise reduction; Shock noise; Supersonic jet noise; Convergent-divergent nozzles	Unclassified - unlimited STAR Category 71

19. Security Classif. (of this report)	20. Security Classif. (of this page)	21. No. of pages	22. Price*
Unclassified	Unclassified		

*For sale by the National Technical Information Service, Springfield, Virginia 22161

National Aeronautics and
Space Administration

Washington, D.C.
20546

Official Business
Penalty for Private Use, $300

SPECIAL FOURTH CLASS MAIL
BOOK

Postage and Fees Paid
National Aeronautics and
Space Administration
NASA-451

NASA

POSTMASTER: If Undeliverable (Section 158
Postal Manual) Do Not Return